POLITECNICO DI TORINO

Department of Mechanical and Aerospace Engineering

MSc Thesis
in Automotive Engineering

Development of simplified vehicle models for impact to barrier

Tutor

Prof. Eng. Alessandro Scattina

Candidate

Simone Saraceno

April 2023

Acknowledgments

At the end of my bachelor's degree, I never thought I would have continued my studies with a master thesis. However, the pandemic forced me to take this journey. Today I can say I'm happy with my choice because I learned all what I expected, and I wanted to learn to become an automotive engineering. In addition, I had the opportunity to meet lots of people with which I shared though and nice moments.

I want to thank a lot of people who was part of my journey, starting from my mom, my dad, my brother, my girlfriend and all my family for their support and for believing in me more than I do. Thank you to all my friends for bearing me and for distracting me from my overthinking.

I would like to thank professor Scattina for his kindness and his encouraging words in my hardest moments. His support helped me growing as a person and as an engineering. I'm also grateful to him for introducing me to my first job experience. I hope I was able to return the favor by being the kind of collaborator he was looking for at the beginning of my thesis work.

Thank you to Dr. Damijan Markovic, Dr. Martin Larcher and the whole JRC team for giving me the possibility to collaborate with them and for inviting me to visit their facilities in Ispra.

Thank you to everyone who believed in me and pushed me to reach my goals.

Simone

April 2023

Abstract

The present thesis, made in collaboration with the European Commission's Joint Research Center (JRC), aims to investigate the reliability and improve the modeling of a N1 vehicle FEM model developed to test barriers for protection of public spaces.

To these aims, two crash sensitivity analysis are conducted using a planar rigid barrier: influence of the angle of impact between vehicle and barrier, and influence of the position of a 1-ton mass placed on the flatbed of the model. While the impact angle has big influence on the exchanged forces and on the momentum, the position of the mass has minor effects.

Then, the model is tested in an impact against a rigid bollard. First, the virtual model is compared with an experimental test of which only the video was available. Extracting the dimensions of the vehicle and of the bollard through reverse engineering, the FEM simulation was set to reproduce the real experiment. A comparison of the kinematic results and of the deformations showed a good correlation between the FEM model and the experimental test. This analysis demonstrated the reliability of the N1 model and its potential to test barriers for protection of public spaces.

Lastly, the same vehicle and bollard have been used to test the influence of the position of the bollard and to compute reaction forces and moments of the bollard central impact.

Index

List of Figures

List of tables

Introduction

The present thesis made in collaboration with the European Research Centre (JRC) [1] has the following objectives:

- Test the reliability and improve the modelling of a FEM vehicle model for virtual testing of barriers for protection of public spaces against vehicle ramming.
- Validate the model making a comparison with a real experimental test.
- Propose a methodology for the computation of reaction forces and moments at the barrier-soil interaction.

The FEM model adopted in this work is the N1 vehicle generic model developed by SVS FEM Services [2] which is freely available (Figure 1) [3].

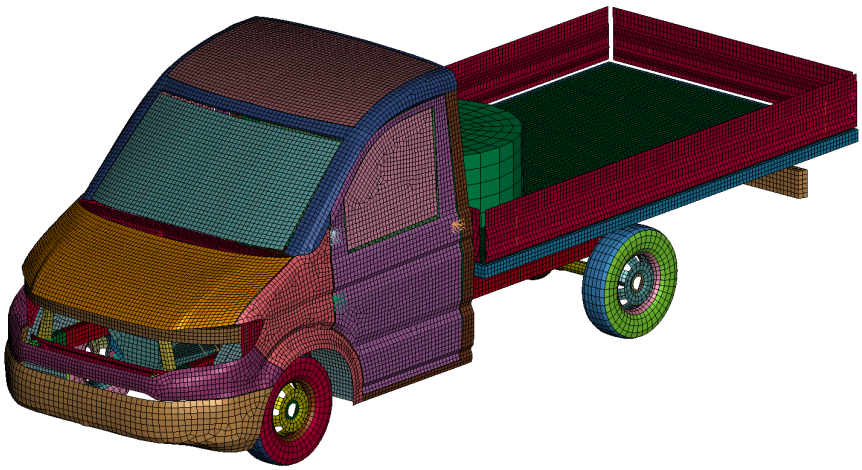

Figure 1. N1 model

It is a simplified vehicle model which has only the necessary structural and exterior components to run fast simulations while ensuring the needed accuracy. Even if it has been designed by reverse engineering on real vehicles, it does not represent a specific model, but the whole category. A rigid cargo (green cylinder) is placed on the flatbed to reproduce a transported good. It is rigidly tied to the flatbed floor to reproduce the restraining system.

The model is organized in numerous includes which are recalled by a main file (Main.k), as shown in Figure 2.

The parameter.k file allows to change the parameters of the vehicle like its dimensions, mass of the components, mass and position of the cargo, suspension stiffness, and initial velocity.

Such parametrization allows to reproduce the dimensions and main characteristics of most existing vehicles belonging to the N1 category.

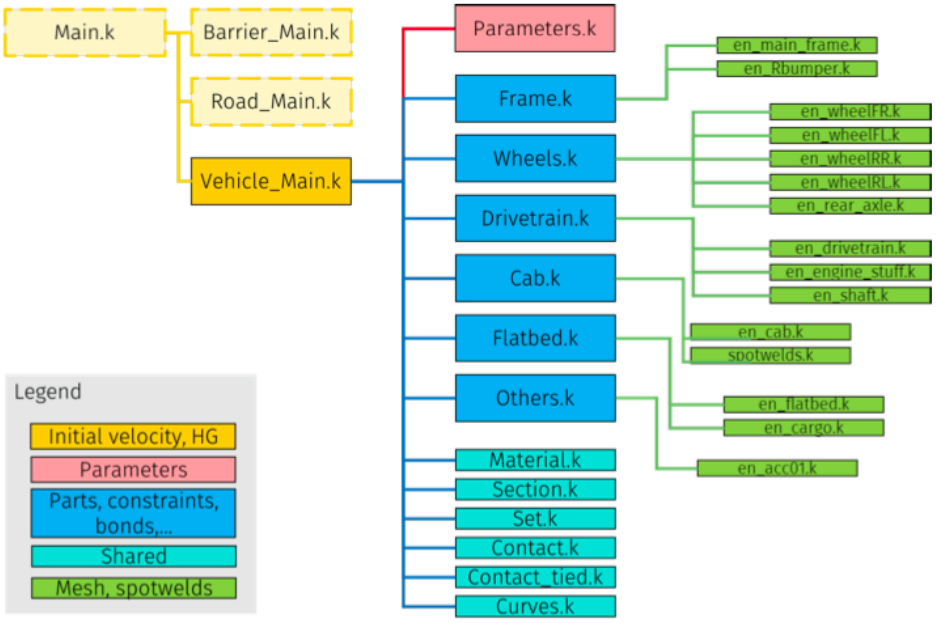

Figure 2. N1 model include organization [4]

In the first chapter, the model is tested in a crash against a rigid planar barrier. A sensitivity analysis is performed on the influence of the angle of impact between the vehicle and the barrier. An additional analysis is made on the friction coefficient to understand its influence on results.

In chapter 2, the same barrier and vehicle setup is used to test the influence of the position of the cargo.

Finally, the model is used to reproduce a bollard impact experimental test. Additional analyses are performed on the influence of the position of the barrier. In the last part of the final chapter, a methodology for the computation of reaction forces and reaction moments of the barrier at the interaction with the soil is proposed.

All simulations carried out with LS-Dyna R12 SMP version (double precision) [5]. Computational resources provided by hpc@polito (http://www.hpc.polito.it).

Chapter 1

Rigid barrier: influence of impact angle

In real crashes it is impossible to have perfect conditions, in which the vehicle impacts the barrier with a perfectly perpendicular inclination. In most cases, the vehicle will impact with a certain angle, changing the force of impact, the energy absorbed by the barrier and many other parameters.

In this chapter, the influence of the angle of impact between the vehicle model and a rigid barrier is analyzed, with the objective of testing the reliability of the model in situations which differs from the perfect one and comparing the deformations of the front structure at each angle. The barrier is made of steel (rigid material) and is modeled with shell elements.

Starting from a barrier parallel to the YZ plane (0° barrier in Figure 3), it is rotated around z-axis in three angle configurations: 5°, 10°, 15°.

In Figure 3, it is possible to see the top view of the model with all the cases analyzed in this section, while in Figure 4 it is possible to see the front view with the dimensions of the barrier.

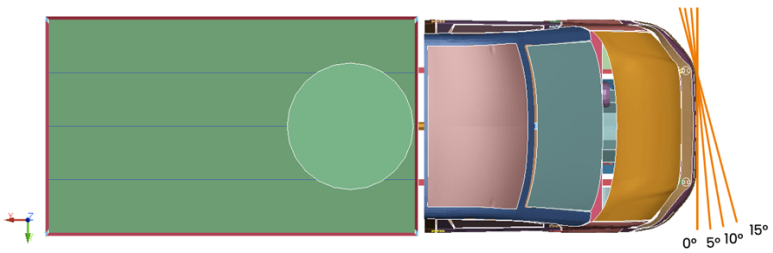

Figure 3. Model setup: inclination of the barrier with respect to the vehicle from top view

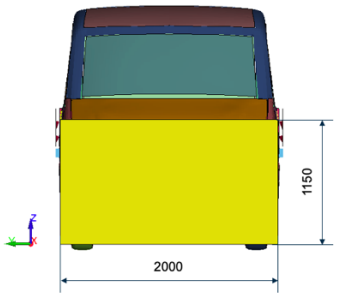

Figure 4. Model setup: front view of the model with barrier dimensions

The vehicle setup is shown in Table 1. Simulations are run with a duration of 1000 ms.

Parameter	Value
Impact velocity (km/h)	56
Barrier-Vehicle friction coefficient	0.6
Cargo mass (kg)	1000
Vehicle length (mm)	6200
Cargo position (mm)	3300

Table 1. Influence of impact angle: vehicle setup

First, an analysis of the animations is made, in order to understand how the vehicle deforms in the different cases, with a particular focus on the deformation of the front longitudinal beams. In the following sections, frame in which the front structure is fully crushed against the barrier (t=100 ms) and the frame at the final instant (t=1000 ms) are shown and discussed.

0-degree barrier

Figure 5 shows the deformation of the 0-degree barrier model, while Figure 6 shows a detail of the deformation of the frame structure. It is possible to see that, both front longitudinal beams bend inward around z-axis; in addition, the longitudinal beams bend also in the central portion and at the rearrest extremity, due to the weight of the cargo.

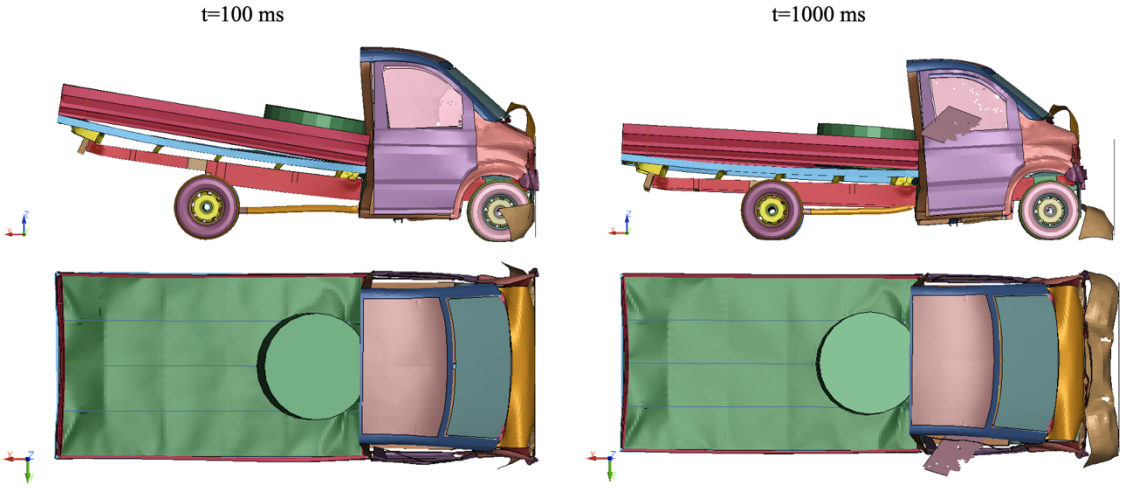

Figure 5. 0-degree barrier: impact at t=100 ms and t=1000s

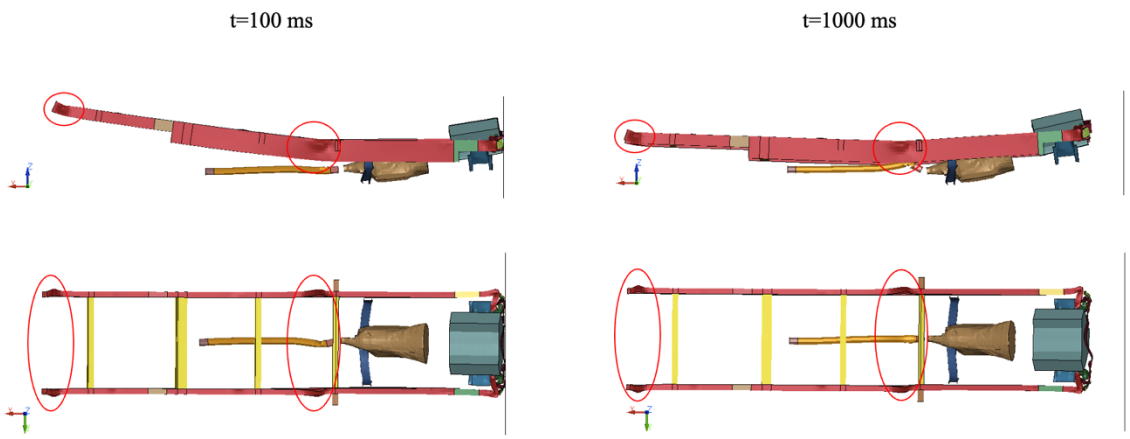

Figure 6. 0- degree barrier: frame detail of the impact at t=100 ms and t=1000 ms

5-degree barrier

The deformation of the whole vehicle is shown in Figure 7, whereas the detail of the deformation of the frame is presented in Figure 8. Even if the angle is small, some differences are appreciable in the deformation of the frame; in fact, while in the 0-degree case both front beams deform inwards, in this case the beam that comes in contact first with the barrier (left beam) bends outward, while the other still deforms toward the inside of the engine bay.

In addition, the vehicle is subjected to a yaw rotation, which is not present in the perpendicular impact.

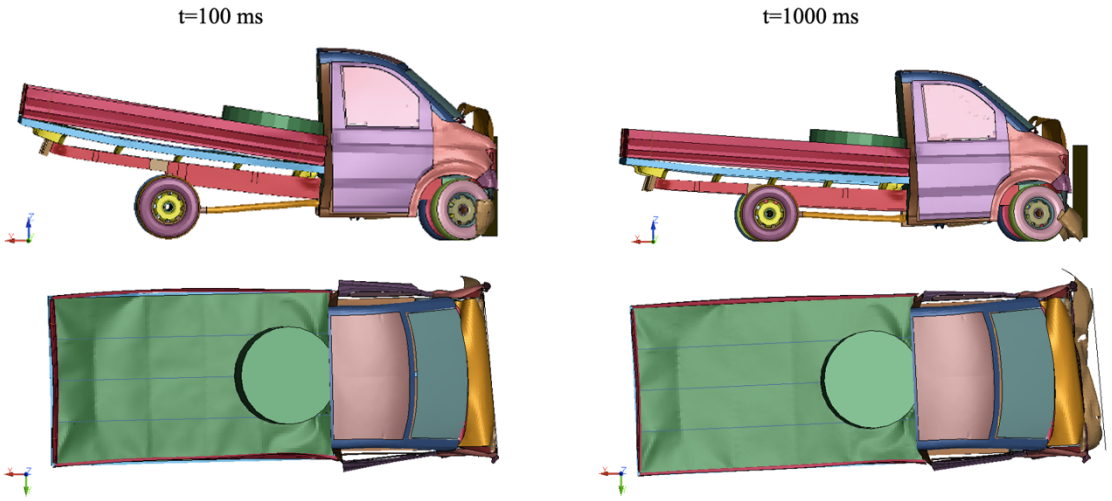

Figure 7. 5-degree barrier: impact at t=100 ms and t=1000 ms

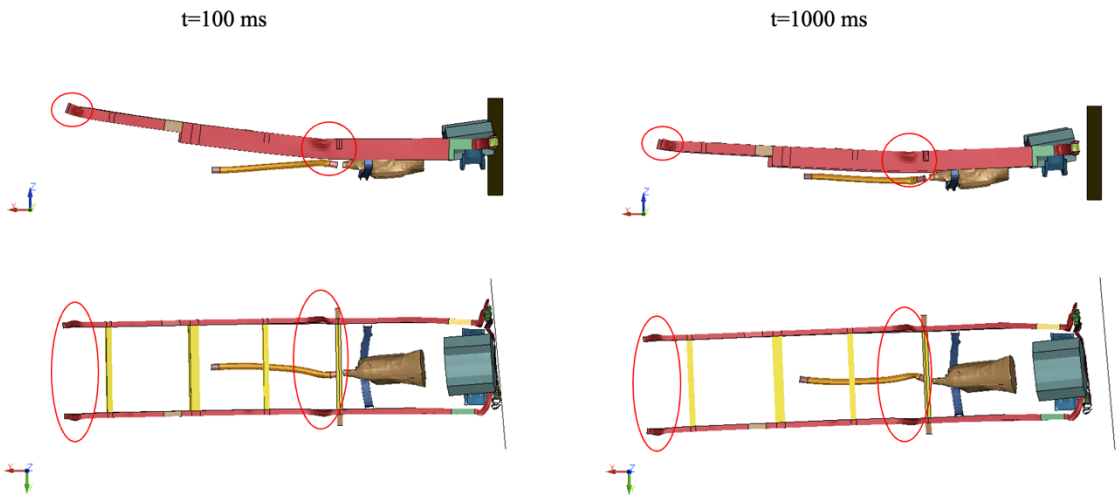

Figure 8. 5-degree barrier: frame detail of the impact at t=100 ms and t=1000 ms

10-degree barrier

Figure 9 shows the deformation of the whole vehicle, while Figure 10 presents the detail of the frame deformation. The longitudinal beams have a different deformation in the central part, which is due to the rotation of the cabin, around z-axis, with respect to the rear part of the vehicle. In the front part, a greater portion of the left longitudinal beams bends with respect to the right one. It is because the left beam comes in contact first against the barrier. In addition, this beam deforms outward, while the right beam deforms inward, as in the previous case.

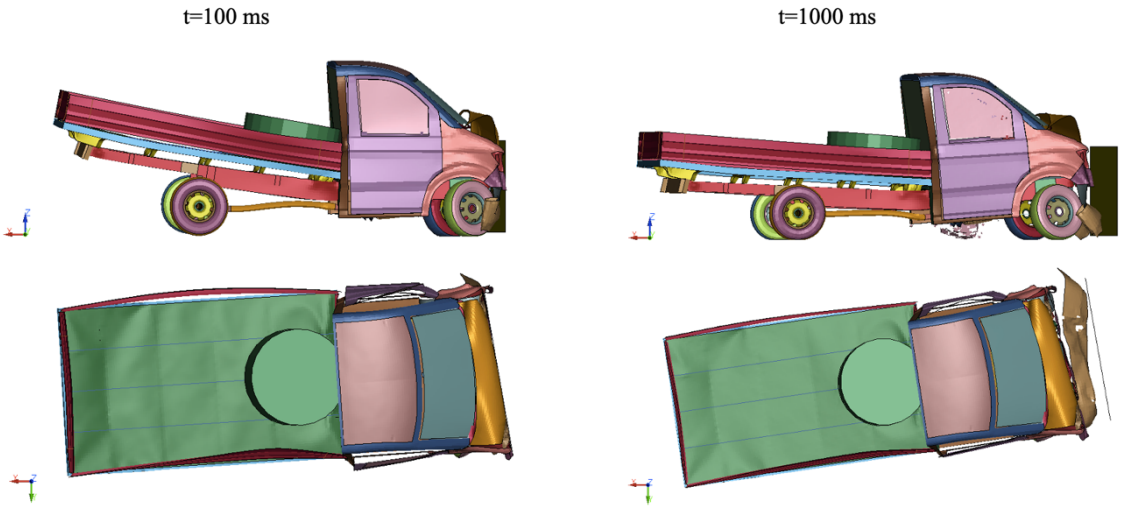

Figure 9. 10-degree barrier: impact at t=100 ms and t=1000 ms

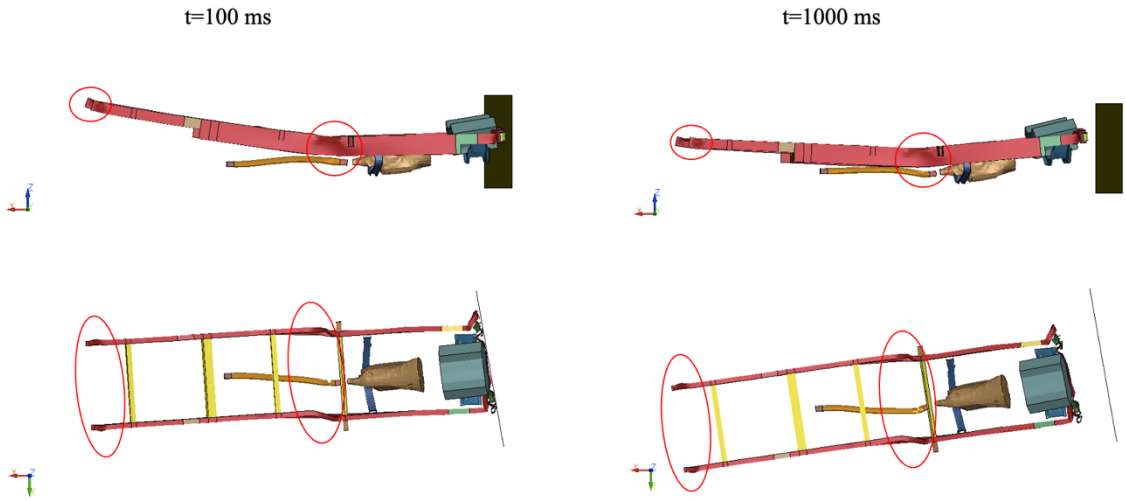

Figure 10. 10-degree barrier: frame detail of the impact at t=100 ms and t=1000 ms

15-degree barrier

In Figure 11 it is possible to appreciate the deformation of the whole vehicle, while in Figure 12 it is possible to see the deformation of the frame. The yaw rotation of the vehicle at the end of the simulation is maximum with respect to the previously analyzed cases. Contrary to the previous cases, the two front beams do not deform in the same way; in fact, only the right beam bends toward the inside, while the left beam has a crushing behavior. Finally, the central part of the frame has a great deformation along the vehicle y-direction.

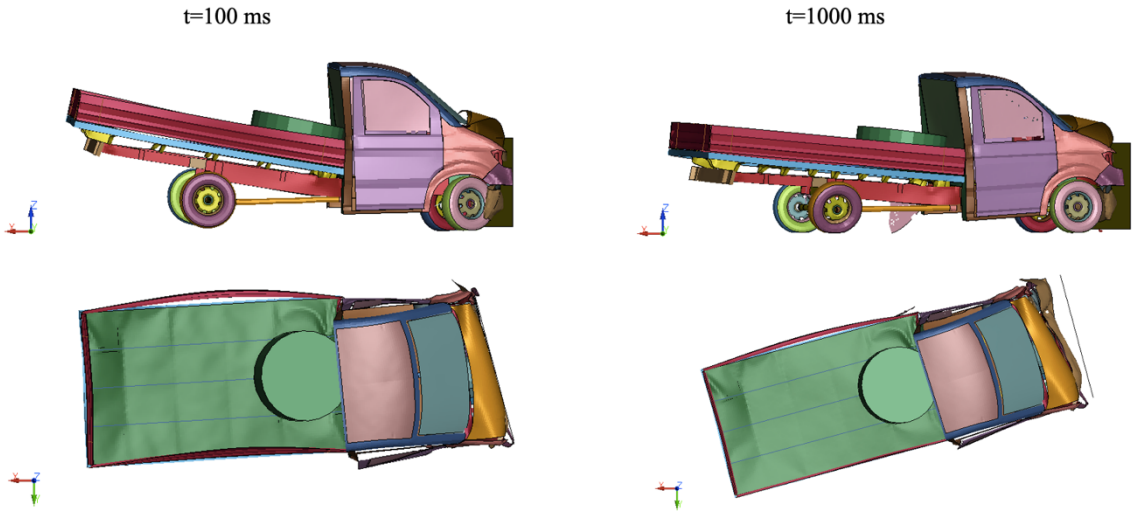

Figure 11. 15-degree barrier: impact at t=100 ms and t=1000 ms

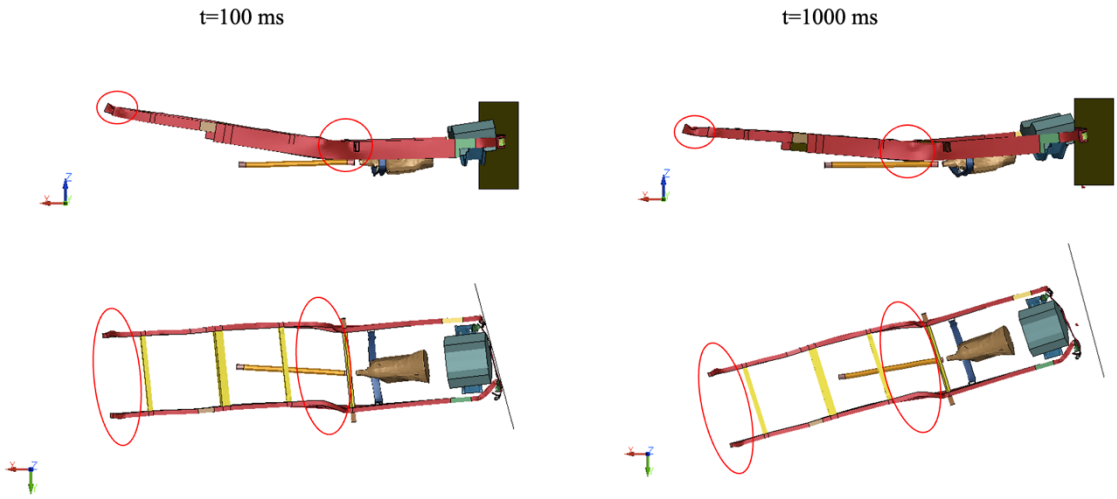

Figure 12. 15-degree barrier: frame detail of the impact at t=100 ms and t=1000 ms

Summing up, changing the angle of impact between the vehicle and the barrier has a great influence on the deformation of the frame and on the overall behaviour of the model.

In particular:

- As the angle increases, a greater yaw rotation of the whole vehicle is appreciated.
- All models show a deformation of the rear part of the longitudinal beams, caused by the weight of the cargo, and its constraints with the flatbed; indeed, being the two parts tied, the cargo tends to lift the flatbed (and the rear axle) when the vehicle arrests, and consequently, the anchorages with the beams are stressed and the deformation is created.
- The central part of the frame shows an increasing deformation along the vehicle y-axis. This phenomenon happens because when the vehicle fully crushes against the barrier, the cabin stops its motion and receives a rotation dictated by the inclination of barrier while the flatbed (with the cargo) still moves along the initial direction. In addition, a deformation in z direction is present again due to the weight of the cargo.
- The front part is heavily influenced by the impact angle, which changes the way front beams deform. In the perpendicular case (0-degree barrier) both beams bend inward, while in the 5-degree and 10-degree simulations, they bend toward the same direction, due to the different time of contact of the beams. Finally, in the 15-degrees simulation, the left beam has a regular crush behaviour instead of bending as in other cases, while the right beam bends inward.

In the following section, the influence of the impact angle on total, kinetic and internal energy is analysed.

Energy components

In Figure 13 it is possible to see the energy components of each case. The total energy has very little differences between all cases. It means that, not only the kinetic energy and the internal energy is almost identical in all cases, but also other energy components, like the hourglass energy, are low enough not to impact on results.

A zoom of the kinetic energy plot between 0 and 0.1 seconds can be seen in Figure 14. It is clear that even changing the angle of impact between vehicle and barrier, results remain almost unchanged. A very little increase in kinetic energy is appreciated in the window between 0.01 s and 0.04 s. However, all curves converge to 0 when the vehicle stops.

Finally, a detail of the internal energy plot between 0 and 0.1 seconds is presented in Figure 15. Also in this case, biggest differences are appreciated in the range 0.01-0.04 seconds. A difference of less than 3% of internal energy is present after 0.1 seconds between the 0-degree barrier case and the 10-degree barrier case. The difference with the 5-degree barrier case and the 15-degree barrier case is even lower.

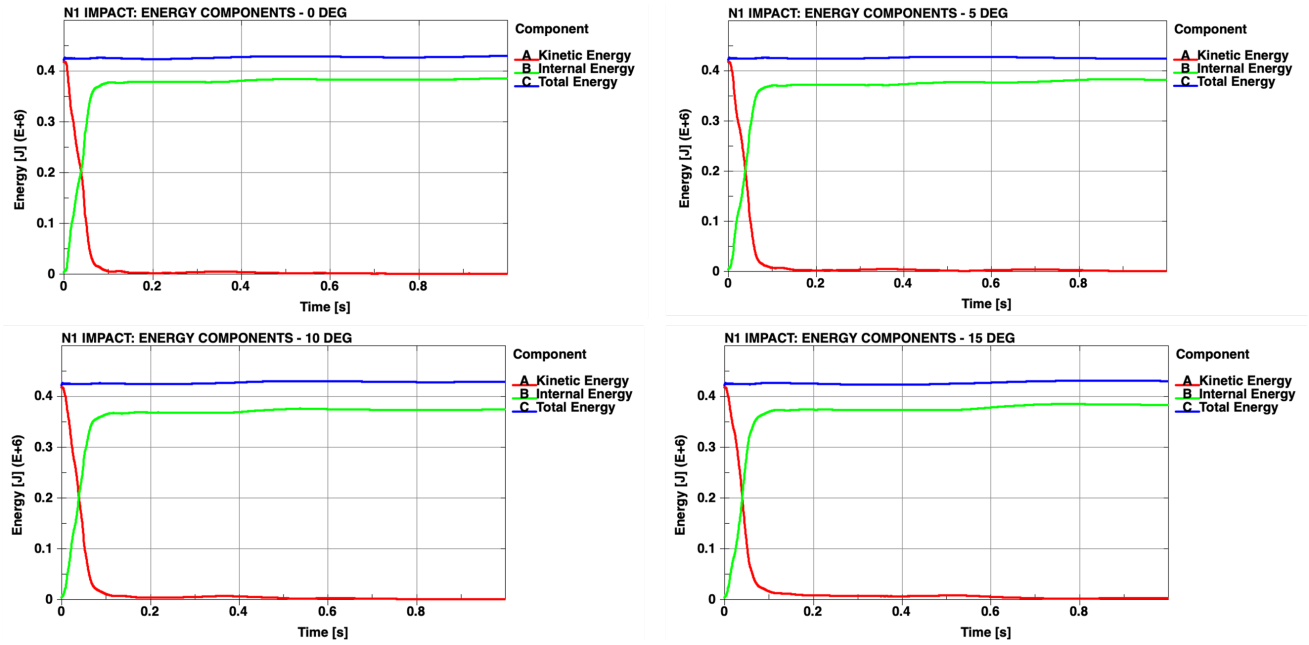

Figure 13. Influence of impact angle: **e**nergy components

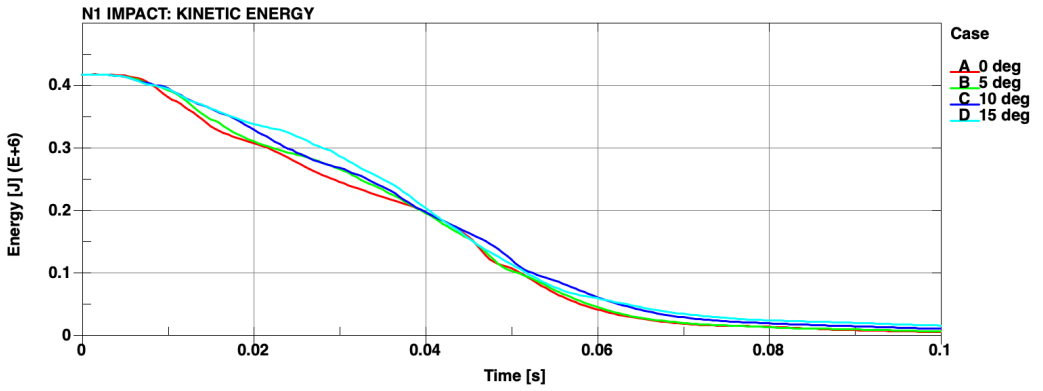

Figure 14. Influence of impact angle: kinetic energy zoom between 0-0.1 s

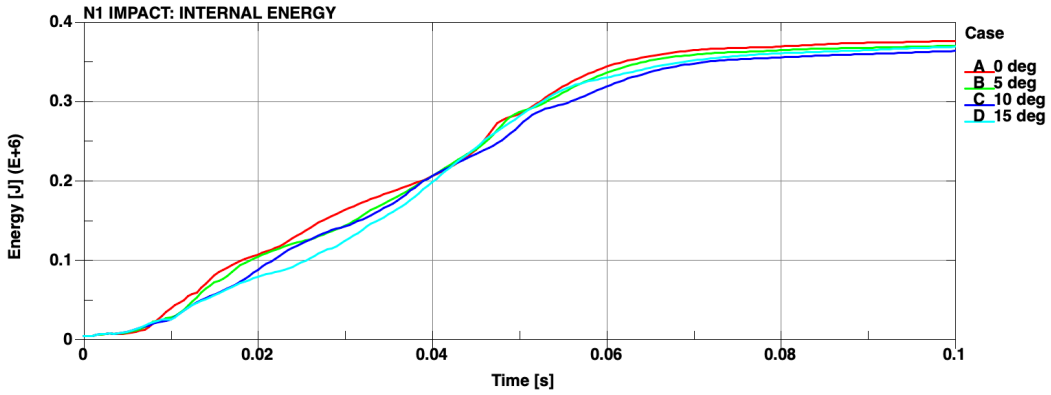

Figure 15. Influence of impact angle: internal energy zoom between 0-0.1 s

In the following section, the plots of the contact force between vehicle and barrier are compared. In the impacts with an angle different from 0, both X and Y force components are generated. For sake of simplicity, the discussion is divided for each component.

Contact force: X component

The X component of the contact force between vehicle and barrier is presented in Figure 16. The first instants coincide with the crushing of the whole front structure of the vehicle, while the peak is generated at the instant at which the engine impacts against the barrier. It is possible to notice that such peak decreases in magnitude and occurs at a longer simulation time as the barrier angle is progressively increased.

The magnitude of the peak reduces because in the 0-degree barrier simulation, the engine contacts all its front surface against the barrier, while in the simulations in which the impact is not perpendicular, a minor contact area is involved.

The different timing of the peak is caused by the change in distance between the engine and the barrier; indeed, being the engine positioned centrally inside the engine bay, increasing the slope angle of the barrier, it gets further and must cover a longer distance to impact.

Finally, it is possible to notice that after 0.1 seconds, the contact force is equal to 0, until the end of the simulation, in all cases. The reason is that after the vehicle fully crushes against the barrier, it bounces back, and they do not contact anymore.

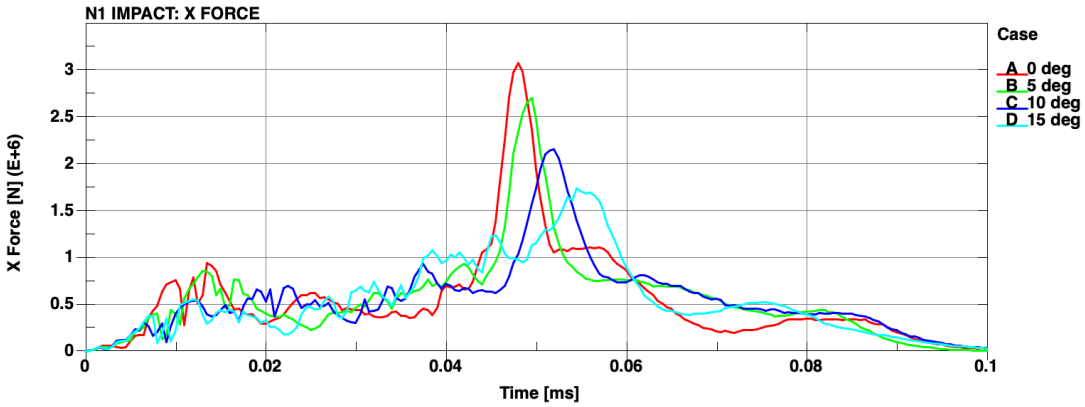

Figure 16. Influence of impact angle: contact force X component

Contact force: Y component

Figure 17 shows the plot the of the Y components of the contact force between vehicle and barrier. It is possible to see that the magnitude is overall lower with respect to the X components of the force.

In the simulation with 0-degree barrier, the Y component is much lower with respect to the cases with inclined barrier.

As the impact angle is increased, the peak Y force increases. However, the two trends are not strictly correlated as with the X component. It is possible to notice that the 15-degree barrier case has a lower peak force with respect to the 10-degree barrier simulation, even if the angle is greater. The reason can be addressed to the different deformation of the front longitudinal beams. While in the 5-degree barrier case and in the 10-degree barrier cases both front beams bend, in the model with 15-degree barrier, only the right beam bend, whereas the left beam crushes, as shown in Figure 18, where it is possible to see the frame at which the peak force arise. This difference changes the way the engine impacts against the barrier, and consequently the peak of the force.

Finally, as in the X force plot, also in this case the maximum of the force occurs at a longer simulation time as the angle of impact increases. The peaks of the X and Y force components arise at the same time.

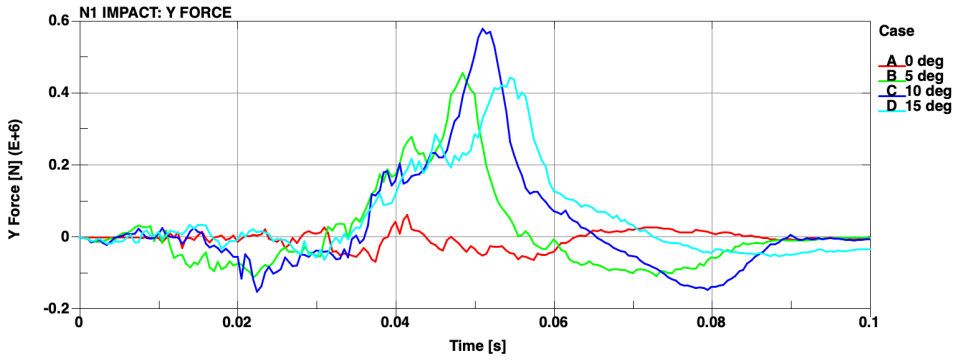

Figure 17. Influence of impact angle: contact force Y component

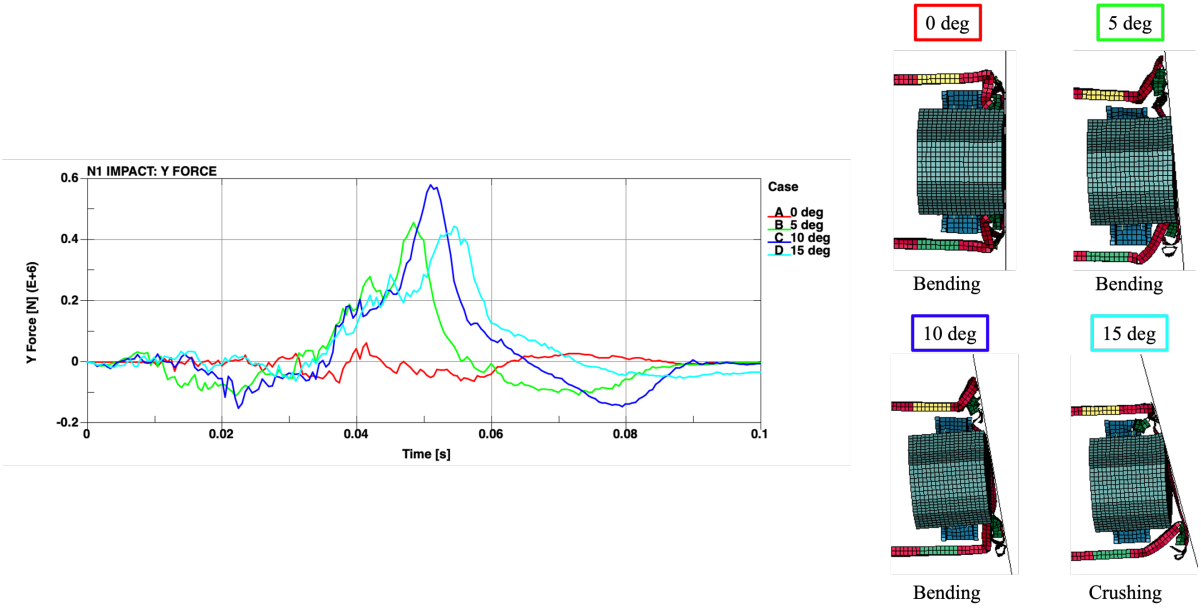

Figure 18. Influence of impact angle: Y force peak comparison

In the following section the total momentum of all components of the vehicle are compared. Both X and Y components are present in the models with inclined barrier, as in the plots of the contact force.

Momentum: X component

X component of the momentum is slightly affected by the angle of impact between vehicle and barrier. In Figure 19 it is possible to see the plots for the whole simulation duration. In all cases the momentum tends to zero. As in the contact force plots, the change in momentum occurs while the vehicle is impacting against the barrier, and then is equal to 0 for the rest of the simulation. For this reason, in Figure 20 a detail window from 0 seconds to 0.1 seconds is shown.

At 0.045 s, the curve of the 0-degree barrier case is steeper than the cases with inclined barrier. The slope reduces increasing the angle of impact. However, this difference is recovered at 0.1 s, where all curves are well overlapped.

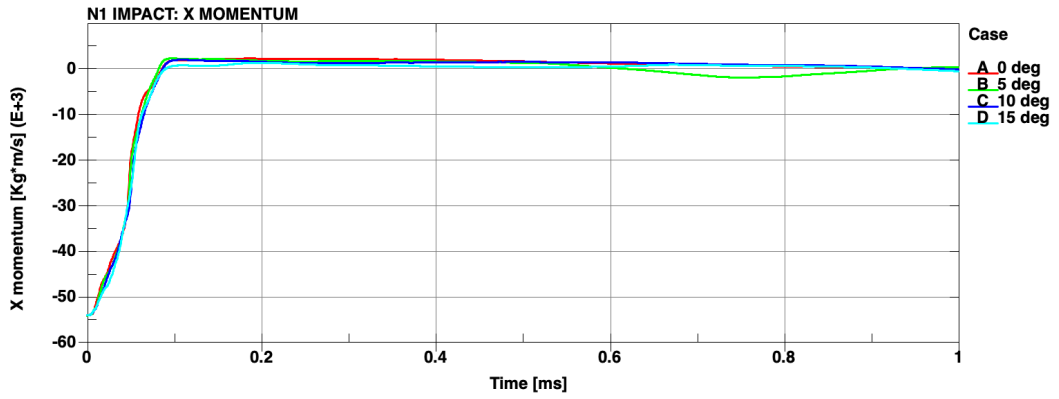

Figure 19. Influence of impact angle: X Momentum plots

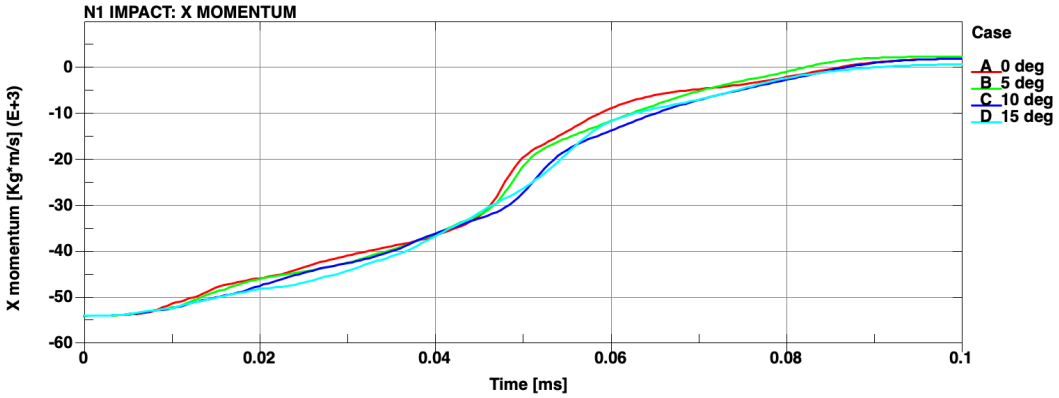

Figure 20. Influence of impact angle: X Momentum plots zoom (0-0.1 s)

Momentum: Y component

Y momentum plot is heavily influenced by the angle of impact; indeed, increasing the angle, the magnitude of the Y component increases. In Figure 21 it is possible to observe this trend.

The curve of the 0-degree barrier model is the lowest one, however it is not equal to 0 because the model is not perfectly symmetric.

In all the other cases, the plot shows a peak around 0.09 s, and then slowly decreases over time. Contrary to the X component of the momentum, in this case curves do not tend to 0 at the end of the simulation (1 s). This behavior is caused by the settling of the vehicle after the impact.

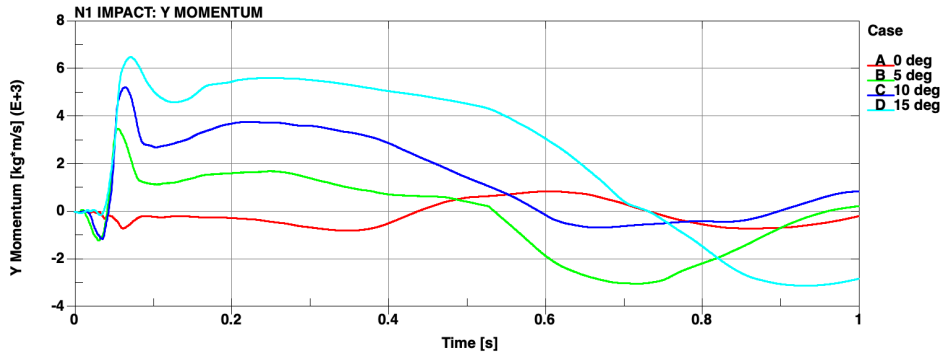

Figure 21. Influence of impact angle: Y momentum plots

Friction sensitivity analysis

In a real experimental test, it is not always possible to determine the influence of all variables with precision, like the friction coefficient between vehicle and barrier. These values are influenced by the materials contacting, the treatment of the surfaces, the dirt present, and many other parameters. However, thanks to N1 FEM model, it is possible to change these values to determine the influence of this parameters in a very fast and easy way.

In this section, the influence of the friction coefficient between barrier and vehicle is analyzed. In the previously shown results, the static and dynamic friction coefficients were set to 0.6, considering that the barrier is made of steel and the front part of the vehicle has both plastic and steel components [6].

Two friction coefficients are compared with previous simulations: 0.2 and 0. For sake of simplicity, only the 0-degree barrier and the 15-degree barrier models are used for the analysis. The setup is equivalent to the one presented in Table 1.

As shown in Figure 22, the friction has poor influence on the perpendicular impact, because there is little-to-no sliding between the vehicle and the barrier.

On contrary, the model with inclined barrier is more affected; indeed, an increase in kinetic energy is experienced in the frictionless case, while the case with friction coefficient equal to 0.2 is contained between the other two curves for the whole simulation. In this case the influence of friction is more evident since the vehicle slides against the barrier during the impact.

In Figure 23 it is possible to see how the internal energy of the 0-degree barrier case is again slightly influenced by friction.

However, the 15-degree barrier model shows a different behavior with respect to the kinetic energy plot. In this case, the curve of the 0-friction case is lower during the impact and then has an increase in internal energy which tends to the same value of the simulation with friction equal

to 0.6. The intermediate case (0.2) maintains the same value reached at the end of the impact (t=0.1 s), which is lower than the two other cases.

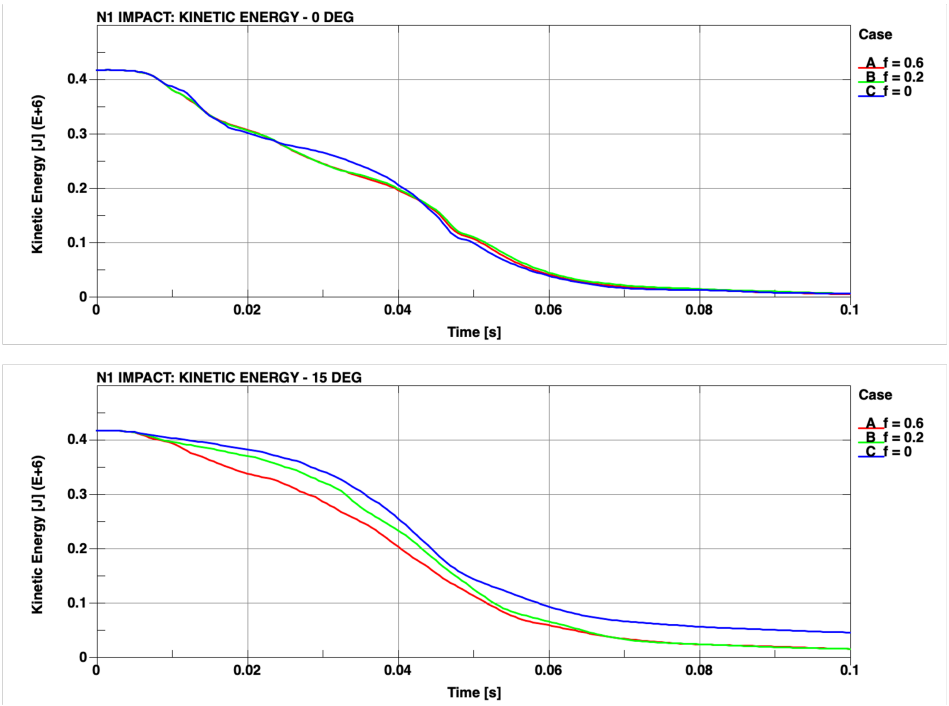

Figure 22. Friction sensitivity analysis: Kinetic energy between 0-0.1 s

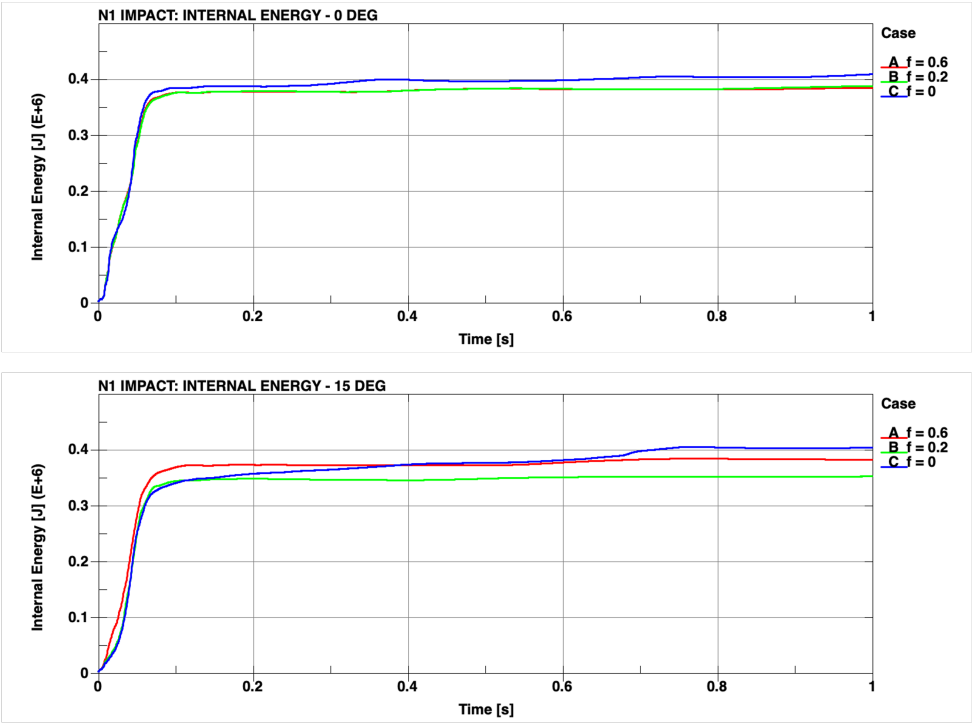

Figure 23. Friction sensitivity analysis: Internal energy

In Figure 24 it is possible to see how the friction coefficient has little influence on the contact force X component of the perpendicular impact.

Bigger differences are present in the inclined model where the sliding between barrier and vehicle anticipates the peak of the force. However, the friction coefficient does not impact on the magnitude.

Figure 25 shows the results of the Y component of the contact force for both cases. In the 0-degree barrier model reducing the friction coefficient, the contact force reduces and becomes almost equal to 0 for the frictionless case.

In the plot relative to the 15-degree barrier case, it is possible to see how reducing the friction, the peak force is anticipated, as for the X component. The magnitude is again very similar in all cases. The peaks of the X component are at the same time of the peaks of the Y components.

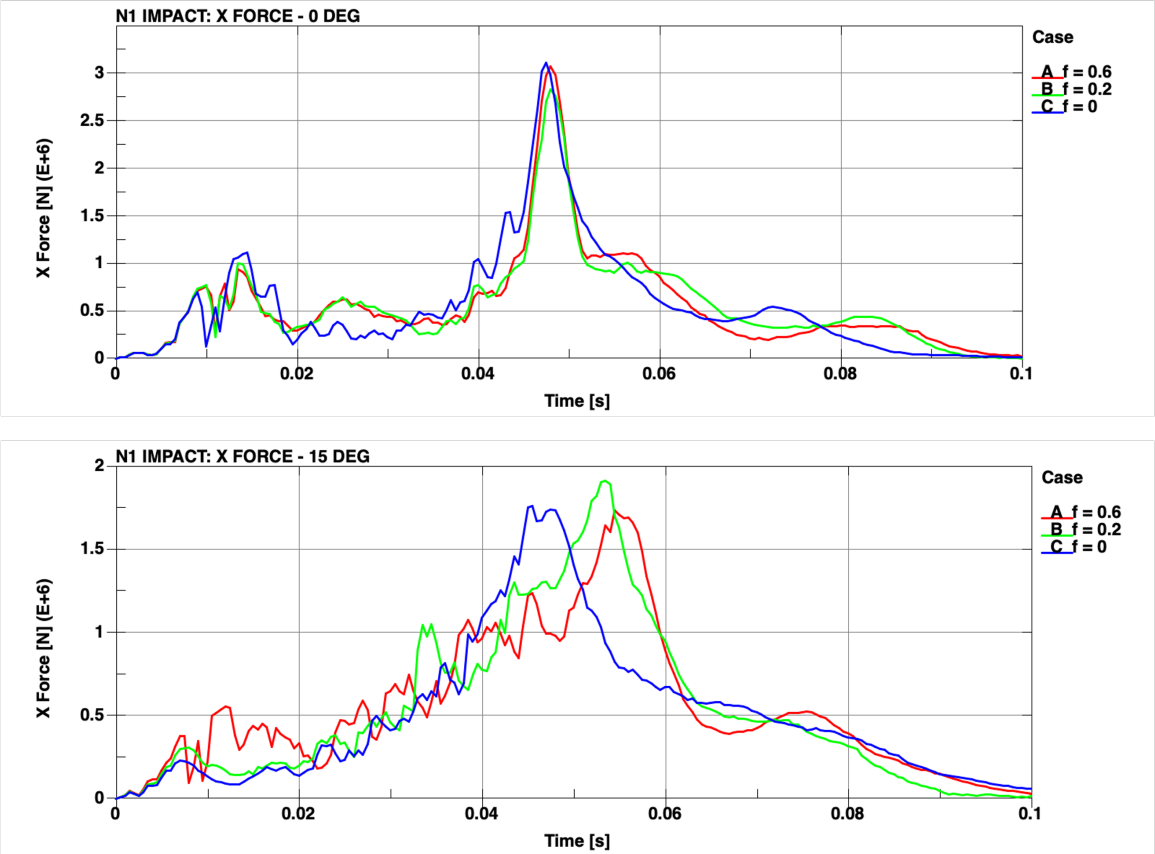

Figure 24. Friction sensitivity analysis: X Force between 0-0.1 s

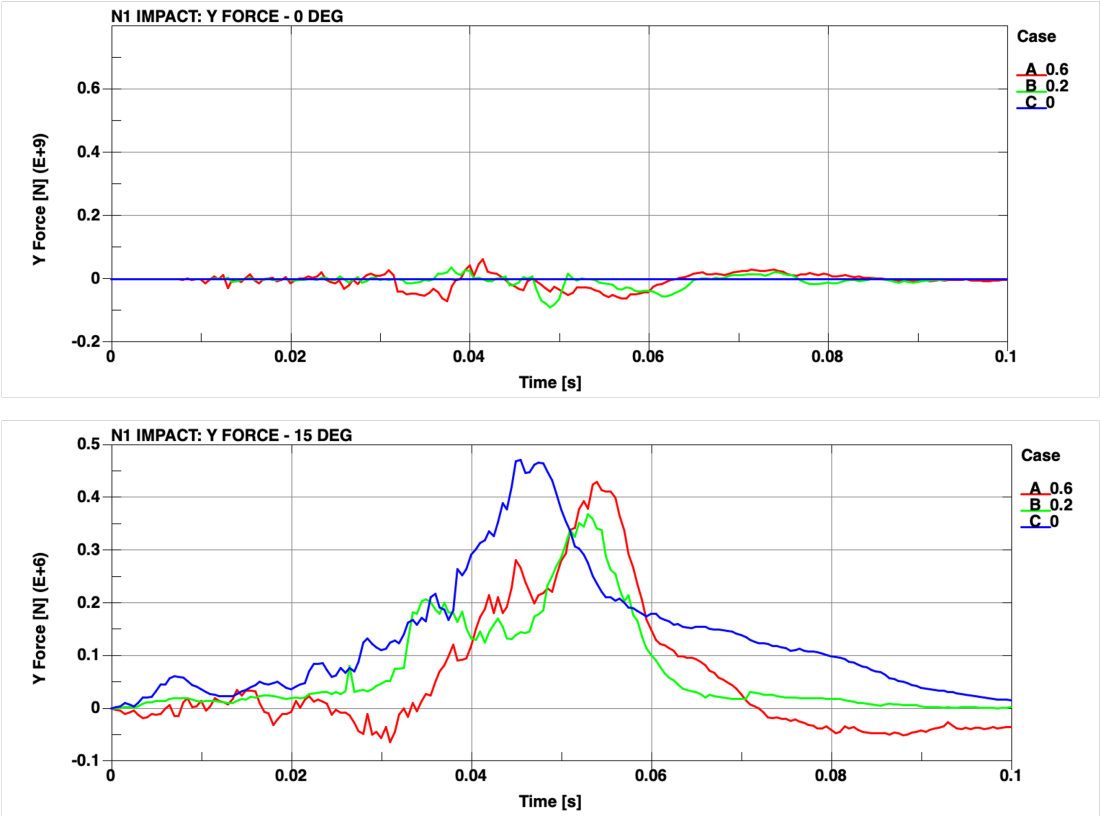

Figure 25. Friction sensitivity analysis: Y force between 0-0.1 s

Momentum plot in X direction is presented in Figure 26. Very little differences are visible in the perpendicular impact, where all curves follow the same trend and are very close for the whole simulation duration.

On contrary, a reduction in momentum is present reducing the friction coefficient for the inclined barrier case. In addition, a slight increase in momentum is present between 0.3 seconds and 0.7 seconds in the frictionless simulations. It is due to the different movement of the vehicle after the impact. However, at the end of the simulation the curve ends at a lower level with respect to the cases with friction.

The 0-degree barrier model has a momentum Y component close to 0 for all the analyzed cases as shown in Figure 27. Very little differences between the curves can be seen in the plot.

The 15-degree barrier simulation has a heavy influence on friction for what the Y momentum is concerned. The absence of friction, double the peak value with respect to the cases with friction. The reason is that being the friction equal to 0, the vehicle slides against the barrier without being decelerated by friction forces. Consequently, a greater speed is experienced in Y direction. However, at the end of the simulation, a minor difference between curves can be seen, even if still present.

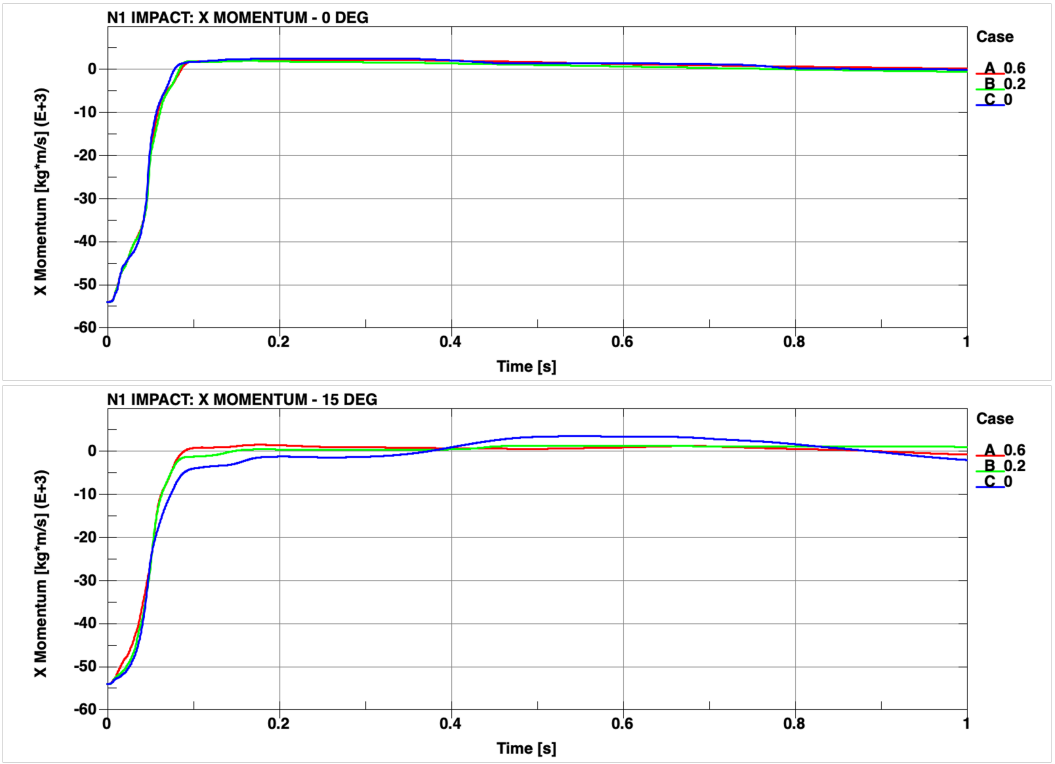

Figure 26. Friction sensitivity analysis: X Momentum

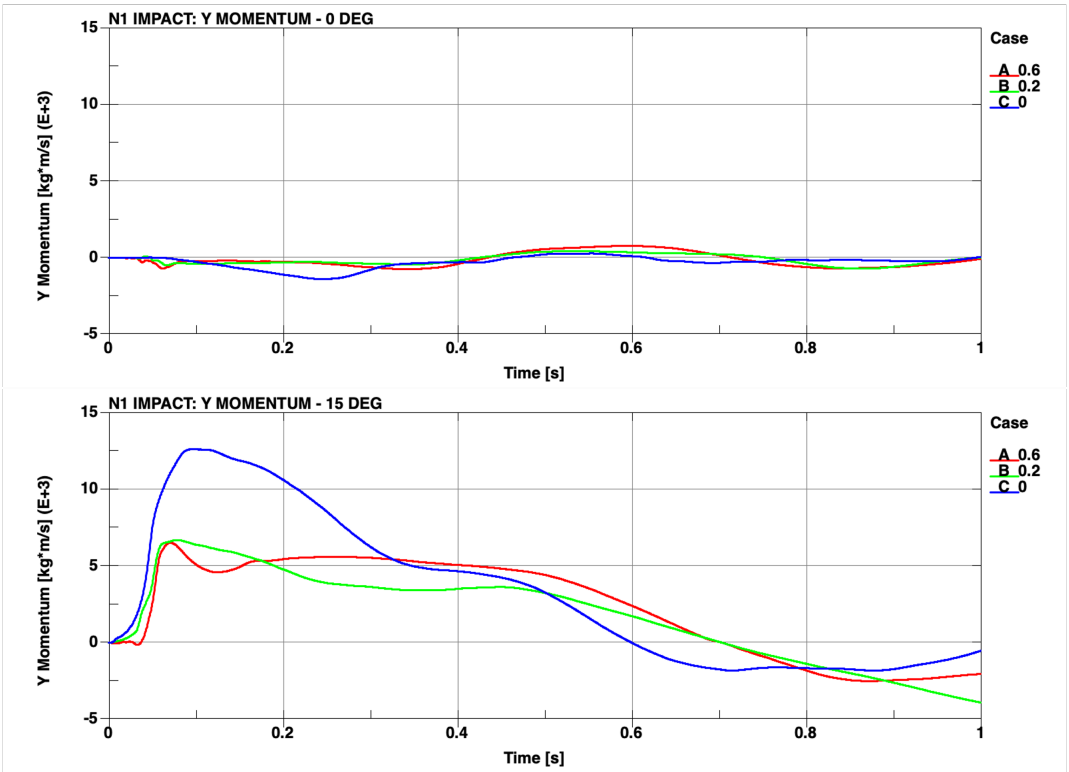

Figure 27. Friction sensitivity analysis: Y Momentum

In conclusion, friction has a great influence only in case of inclined barrier since it changes the sliding between vehicle and barrier and consequently the contact force and the momentum in both X and Y directions. Minor changes can be seen in the exchanged energies.

In case of perpendicular impact, very little differences can be seen in the energy and momentum plot, while a more evident influence is present in the contact force in both X and Y directions.

Force normal to barrier computation

The present section is dedicated to the computation of the contact force component normal to the barrier for the cases with inclined barrier. In particular, it is analyzed the possibility of predicting such force using the X component of the contact force of the model with perpendicular barrier (which is coincident to the force normal to the barrier in this case) multiplied by the cosine of the angle of inclination of the barrier with respect to the vehicle.

In LS-PrePost [7], there are no specific tools or functions implemented to obtain the contact force normal component during the post-processing phase. However, this force is well approximated by the resultant of the contact force.

To test the validity of the correlation between resultant force and normal force, the real forces normal to the barrier were compared to the resultant forces of each case with inclined barrier. To obtain the normal force, the models have been rotated around Z-axis, in the pre-processing phase, to have the normal to the barrier coincident with the global x-axis. In this way, the normal force coincides with the X component of the contact force from the output file. The rotated models are shown in Figure 28.

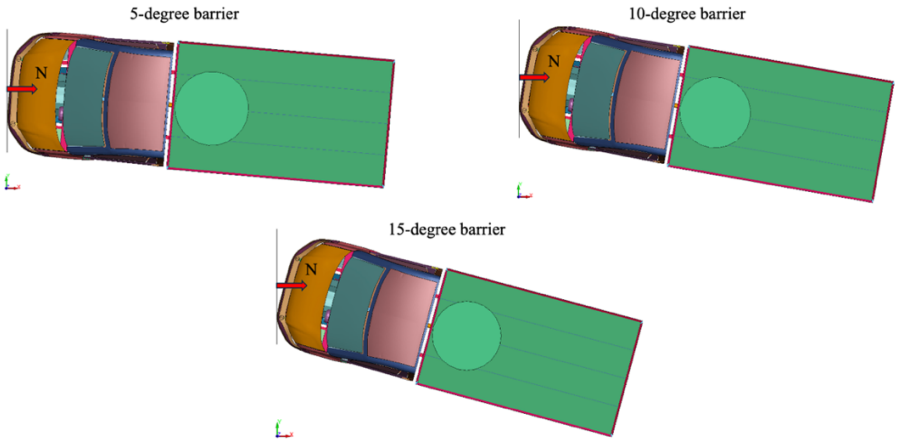

Figure 28. Rotated models for force normal to barrier computation

Results shows a good correlation between the resultant force curve of the cases analyzed in the previous sections (inclined barrier), and the X force of the rotated models shown in Figure 28 (inclined vehicle). The comparison between the two curves can be seen in Figure 29 for all cases with inclined barrier. For the 5-degree barrier and 10-degree barrier simulations, the only difference is the peak force. In the 15-degree barrier model the difference between resultant force and force normal to barrier is greater, but still small enough to be acceptable. These differences are mainly caused by friction. Running the same model without friction, the differences between resultant force of the original models and normal force of the rotated models are eliminated. In the following, results are taken from the original models and not from the rotated models since they were used for all the other analysis.

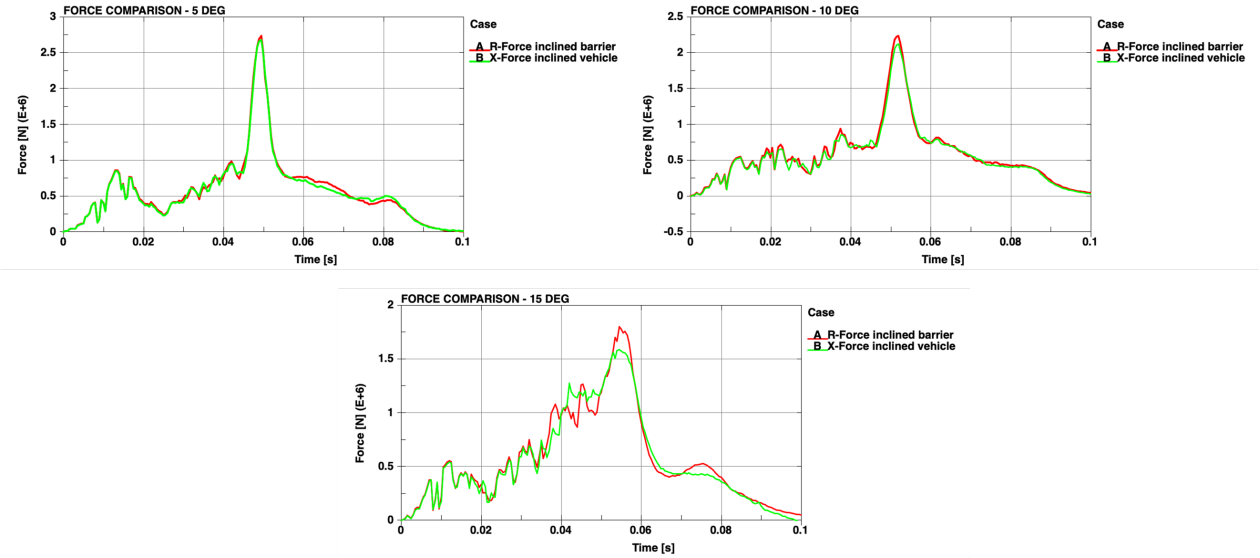

Figure 29. Force normal to barrier computation: resultant force and normal force comparison

The comparison between the normal force of the perpendicular impact, the product between such force and the cosine of the angle of inclination of the barrier, and the resultant force of the cases with inclined barrier is shown in Figure 30.

The prediction made using the normal component of the force of the 0-degree barrier case has low reliability. As the angle of impact is increased, the green (X component of the contact force of the 0-degree case multiplied the cosine of the angle of each case) and the blue (resultant contact force) curves gets more and more different.

Not only the magnitude is different, but also the time at which the peak force occurs, which coincides with the time at which the engine contacts the barrier.

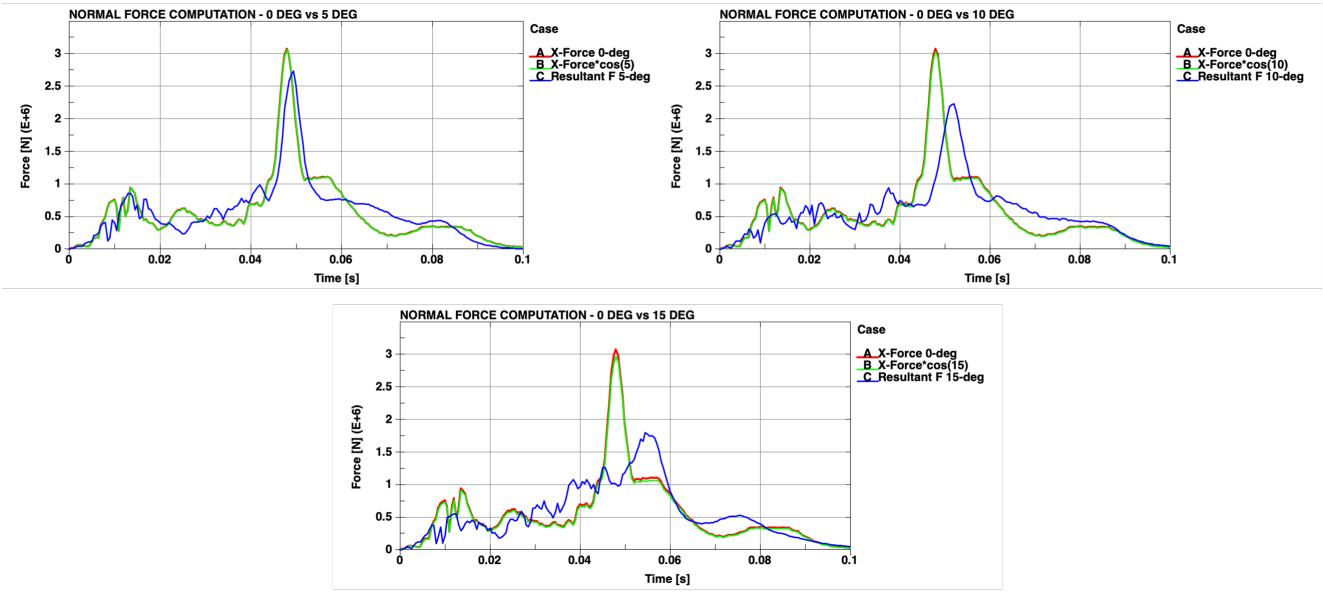

Figure 30. Force normal to barrier computation: force normal to barrier prediction

Chapter 2

Rigid barrier: cargo position influence

When carrying goods on a vehicle of this category (N1), it is important to position and fix them so that they do not move and do not influence the driveability of the vehicle. If many objects are carried, they must be evenly positioned so that they occupy as much as possible the available space and do not become too high.

However, there are no specific regulations about the distribution of the mass. The only rules are that the axle maximum load declared by the constructor must not be exceeded, the loads must be arranged so that the minimum height is maintained, and the objects must be restrained not to move during travelling [8]. In Italy, the maximum permitted weight for each drive and non-drive axle is 12 tons [9]. This limit is imposed to avoid too much load on the road.

In this chapter, the influence of the position of the cargo on the overall behaviour of the model is analysed.

The same rigid barrier used in the previous chapter is adopted for the present analysis with a 0-degree inclination with respect to the vehicle.

Six different cargo positions are analysed. Each configuration is shown in Figure 31. The position of the cargo with respect to the reference frame is expressed in millimetres. The cases with the cargo position in negative y position are not considered since the model is almost perfectly symmetric.

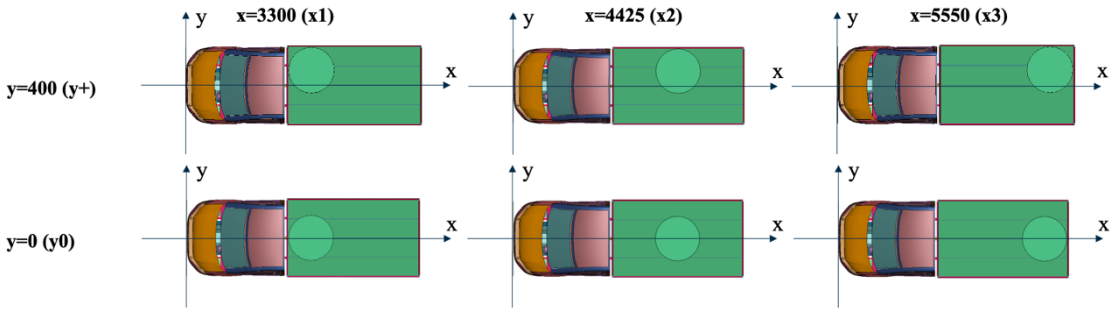

Figure 31. Model setup: cargo positions on the flatbed (in mm)

The vehicle dimensions and the starting conditions of the simulation can be seen in Table 2.

Parameter	Value
Impact velocity (km/h)	56
Barrier-Vehicle friction coefficient	0.6
Cargo mass (kg)	1000
Vehicle length (mm)	6200
Wheelbase (mm)	3280

Table 2. Cargo position influence: vehicle dimensions and initial conditions

Simulations are run with a duration of 1000 ms. In addition, with respect to the original model, contacts were added between the cargo and the flatbed sides, since in the configurations with cargo at y=400 mm, the two parts get in touch.

In the following sections, the animation frame of the vehicle fully impacted against the barrier (t=100 ms) is shown and commented for each case.

Cargo in x1 position

When the cargo is positioned near the cabin, the rear part of the vehicle is lifted during the impact as shown in Figure 32. This motion, caused by the cargo, deforms the central part of the longitudinal beams and the rearrest end of the frame as can be seen in Figure 33.

However, little differences are present between the two cases. The only difference is a slight yaw rotation in the case with cargo placed in “y+” position, which becomes more present toward the end of the simulation. However, the overall deformation of the two cases is very similar.

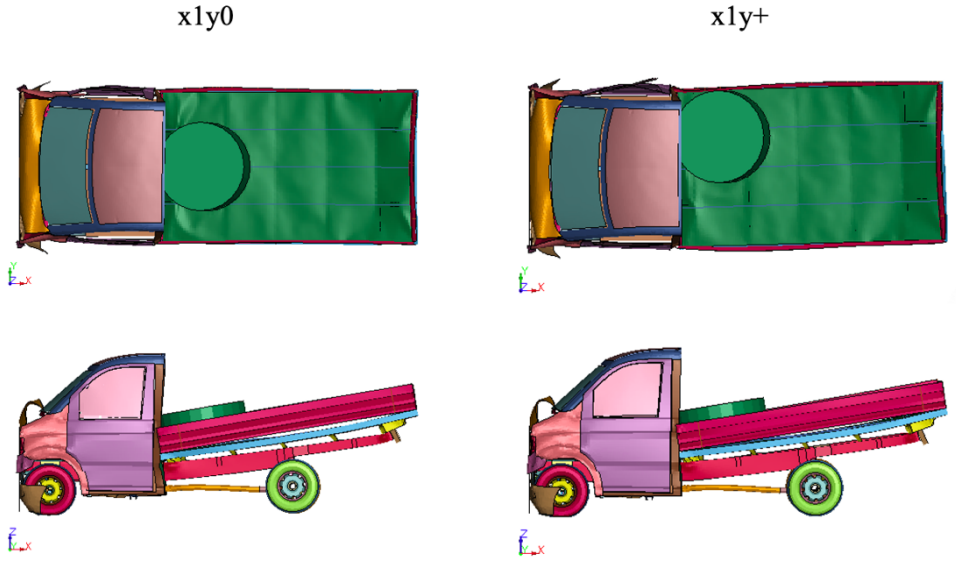

Figure 32. Cargo position influence: vehicle impact with cargo in position x1 at t=100 ms

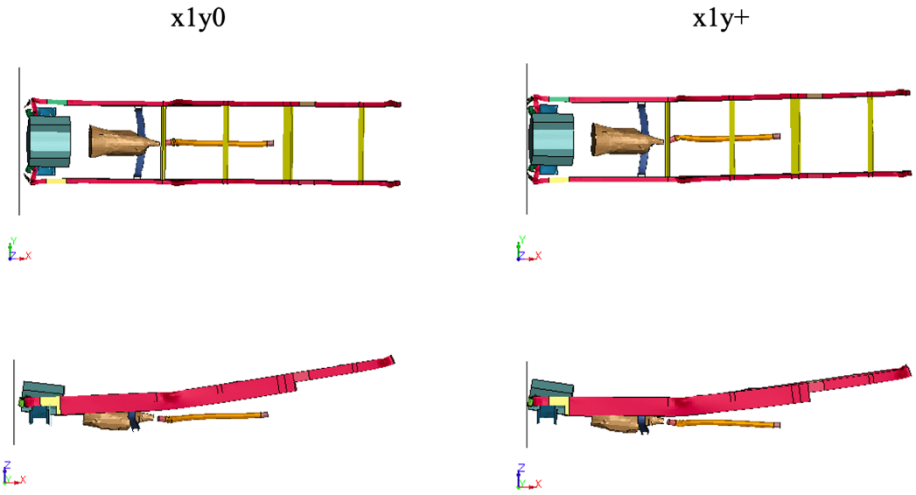

Figure 33. Cargo position influence: frame detail with cargo in position x1 at t=100 ms

Cargo in x2 position

Moving the cargo in the central part of the flatbed, has a big impact on the deformation of the flatbed and reduces the lift of the rear axle (Figure 34). The crossbeams present under the cargo collapses due to its weight, causing an overall different deformation of the frame with respect to the previous case, as presented in Figure 35. No differences are seen in the deformation of the front longitudinal beams, while a lower deformation of the central part can be seen. In addition, in the case with the cargo in position "y+", a slight yaw rotation is appreciated, and a greater deformation along z-axis of the right beam is present with respect to the left beam.

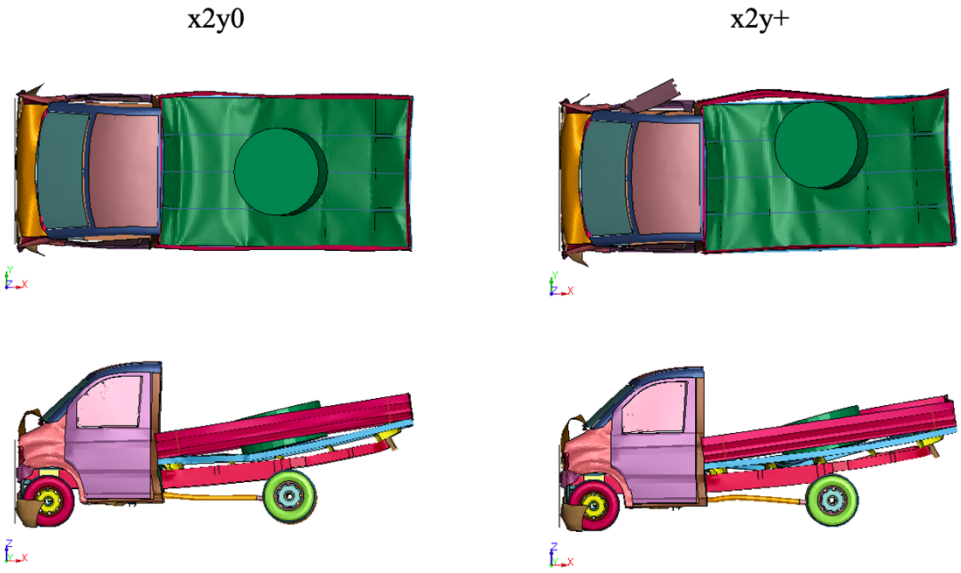

Figure 34. Cargo position influence: vehicle impact with cargo in position x2 at t=100ms

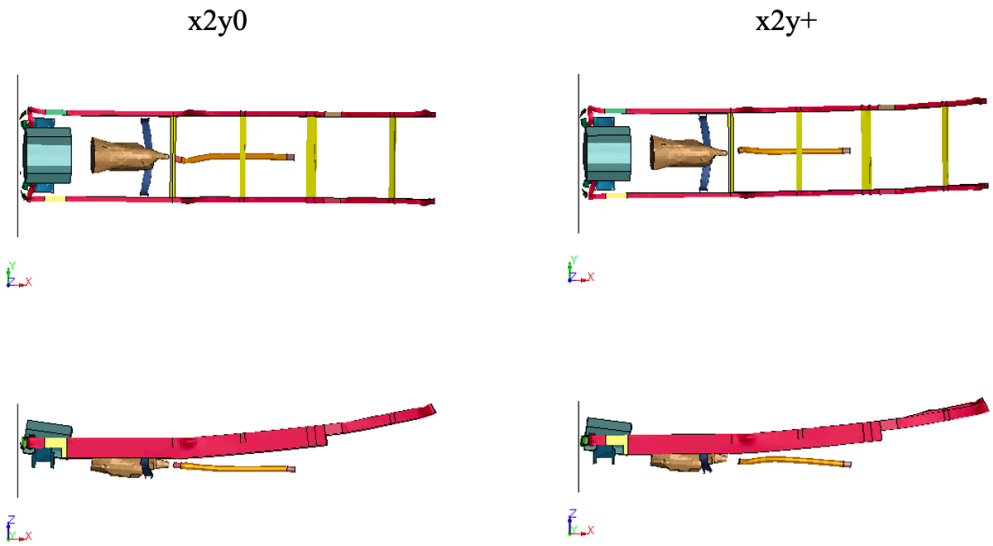

Figure 35. Cargo position influence: frame detail with cargo in position x2 at t=100 ms

Cargo in x3 position

Placing the cargo at the end of the flatbed (x3), has the biggest impact on results among all the analyzed cases. The deformation of the flatbed is maximum, as well as the deformation of the last part of the longitudinal beams (Figure 36). The analysis of the frame deformation (Figure 37) reveals a small deformation in the central part of the longitudinal beams, but a huge deformation in correspondence of the position of the cargo. In addition, when the cargo is not centered on the x-axis (y+), it bends the beam it lays on (right beam in this case) towards the inside of the vehicle.

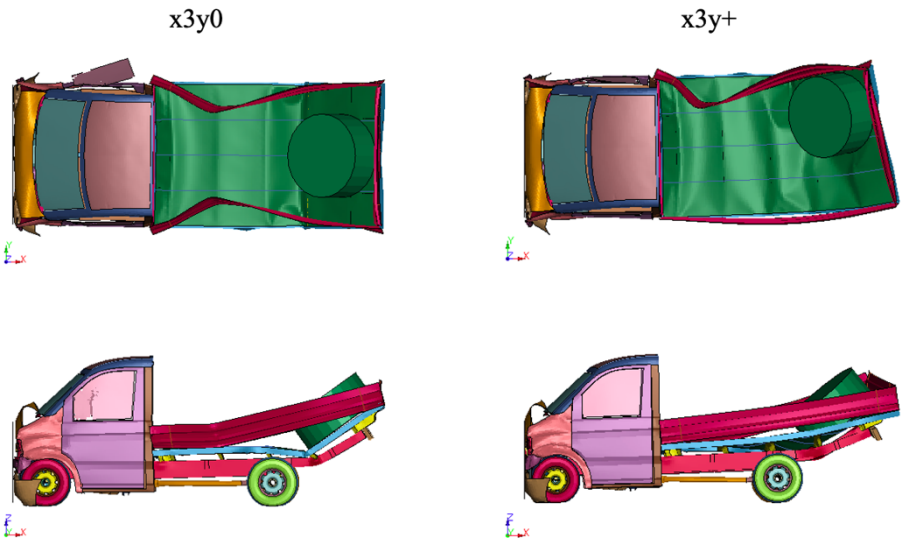

Figure 36. Cargo position influence: vehicle impact with cargo in position x3 at t=100 ms

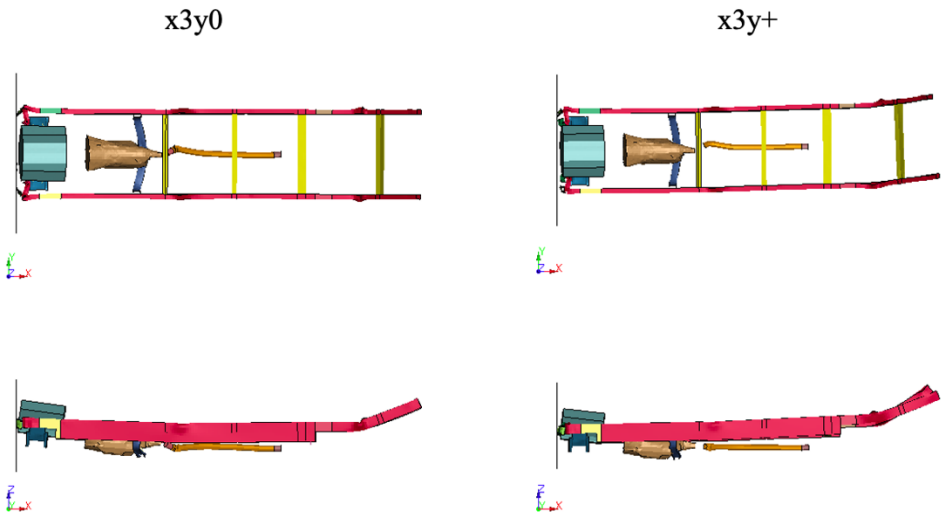

Figure 37. Cargo position influence: frame detail with cargo in position x3 at t=100 ms

In the simulations with the cargo in positions x1 and x2, after the impact the vehicle has a behavior similar to the one explained in the previous chapter. On contrary, when the cargo is positioned at the end of the flatbed (x3), a different behavior can be seen. In Figure 38 it is possible to see the video frame corresponding to the last instant of the simulations with cargo in position x1 (results are similar for the x2 cases), while in Figure 39 it is possible to see the same frame from the x3 simulations.

In the first image the vehicles are settling without getting any further from the barrier and all tires are in contact with the ground. When the cargo is decentered, a slight rotation of the whole vehicle is seen around z-axis with respect to the centered case, where the vehicle remains aligned to x-axis.

In Figure 39, the vehicle is accelerating backward with its front axis lifted. This behavior is more marked in the model with cargo centered on the x-axis (x3y0) but is present also in the simulation with decentered cargo. It starts just after the front part of the vehicle is fully crushed on the barrier. The front axis lifts and the whole vehicle starts to accelerate in the direction opposite to the initial one.

In addition, when the cargo is in position x3y+, the vehicle has an evident yaw rotation, which is greater with respect to the x1y+ case, where this rotation is smaller. This yaw rotation of the x3y+ case limits the backward acceleration. Indeed, it is possible to see that comparing the last instant of the two cases with cargo in position x3 (Figure 39), the vehicle is further from the barrier in the figure on the left, while it is moving in both x and y directions in the decentered case.

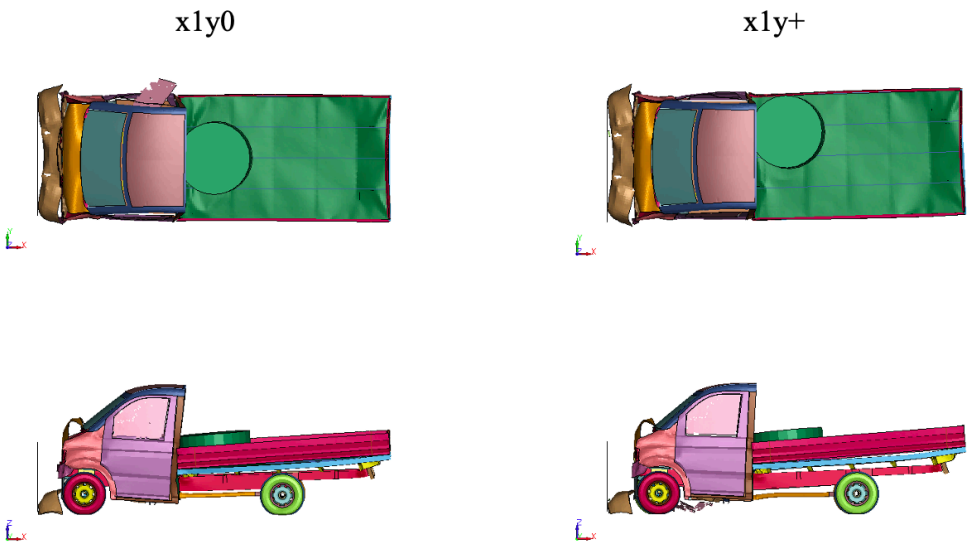

Figure 38. Cargo position influence: vehicle behavior with cargo in position x1 at t=1 s

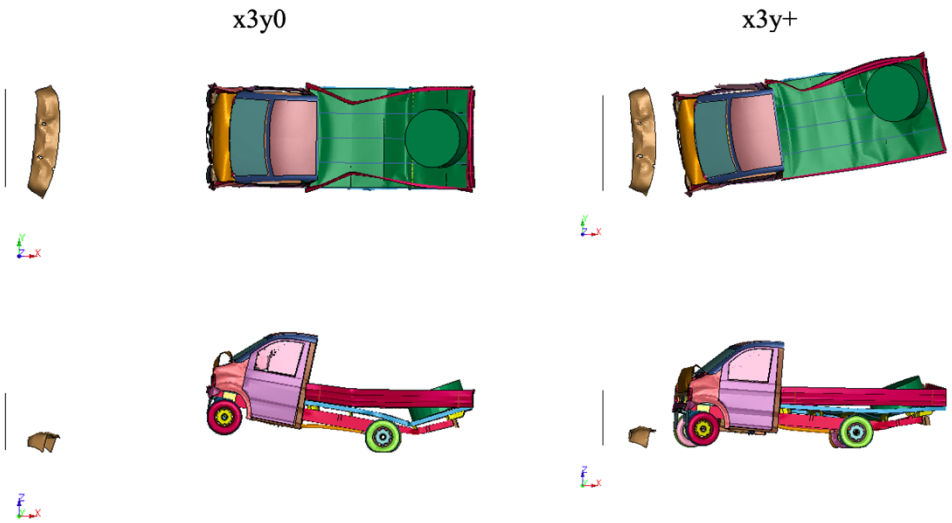

Figure 39. Cargo position influence: vehicle behaviour with cargo in position x3 at t=1 s

In conclusion, when the cargo is placed before the rear axle (x1 and x2), the frame deforms in a similar way in all cases, independently if it is centered on the vehicle x-axis, or placed close to the flatbed side. Both front longitudinal beams bend toward the inside of the engine bay, while a deformation is present in the central portion and at the rearrest end, both caused by the weight of the cargo.

On contrary, when the mass is placed at the end of the flatbed, it creates a great deformation of both the flatbed and longitudinal beams last portion. In addition, a different response of the

vehicle is seen after the impact, where the vehicle starts to accelerate backward and its front axis lifts.

Energy components

In this section, the influence of the position of the cargo on total, internal and kinetic energies involved in the crash are analyzed.

In Figure 40, it is possible to see the graphs for each simulation. The plots of the x1 and x2 cases are very similar, for both centered and decentered cargo. Negligible differences are seen in the total anergy as well as in the kinetic and internal energy. Moving the cargo along x or y axis does not influence the total internal energy absorbed by the vehicle during the impact. During the impact, the kinetic energy is converted into internal energy, and after the impact (after t=0.1 s), both energies remain constant until the end of the simulation. As a consequence, the total energy is constant during the whole simulation.

In the two graphs on the bottom, it is possible to see the plots of the simulations with cargo in position x3. In the centered case (x3y0), the backward acceleration is put in evidence by the kinetic energy increase after 0.2 s. As a result, the total energy increases with the same trend.

Contrary to the previous cases, the kinetic energy is converted into internal energy only during the impact. At the end of the crash event (0.1s), the internal energy remains constant while the kinetic energy increases again due to the acceleration of the vehicle.

In the decentered case (x3y+), a minor kinetic and total energy increase is observed. The reason is the lower acceleration of the vehicle.

In the x3y0 simulation, the two beams are charged like springs by the weight of the cargo. Their accumulated energy is released and the backward acceleration phenomenon arises.

The same behavior is present in the x3y+ case, but the two longitudinal beams do not charge in the same way of the centered case because the cargo deforms the two parts in a different way, being the mass distribution asymmetric in this case. So, less energy is accumulated by the longitudinal beams and a smaller acceleration is created.

In conclusion, the position of the cargo has poor influence on the exchanged energies only up to the end of the crash event. Kinetic, internal and total energy are similar in all cases until 0.2 s, then in the models with cargo in x3 position, an acceleration starts to arise, with a consequent increase in kinetic and total energy. In the other cases, the total energy is constant for the whole simulation.

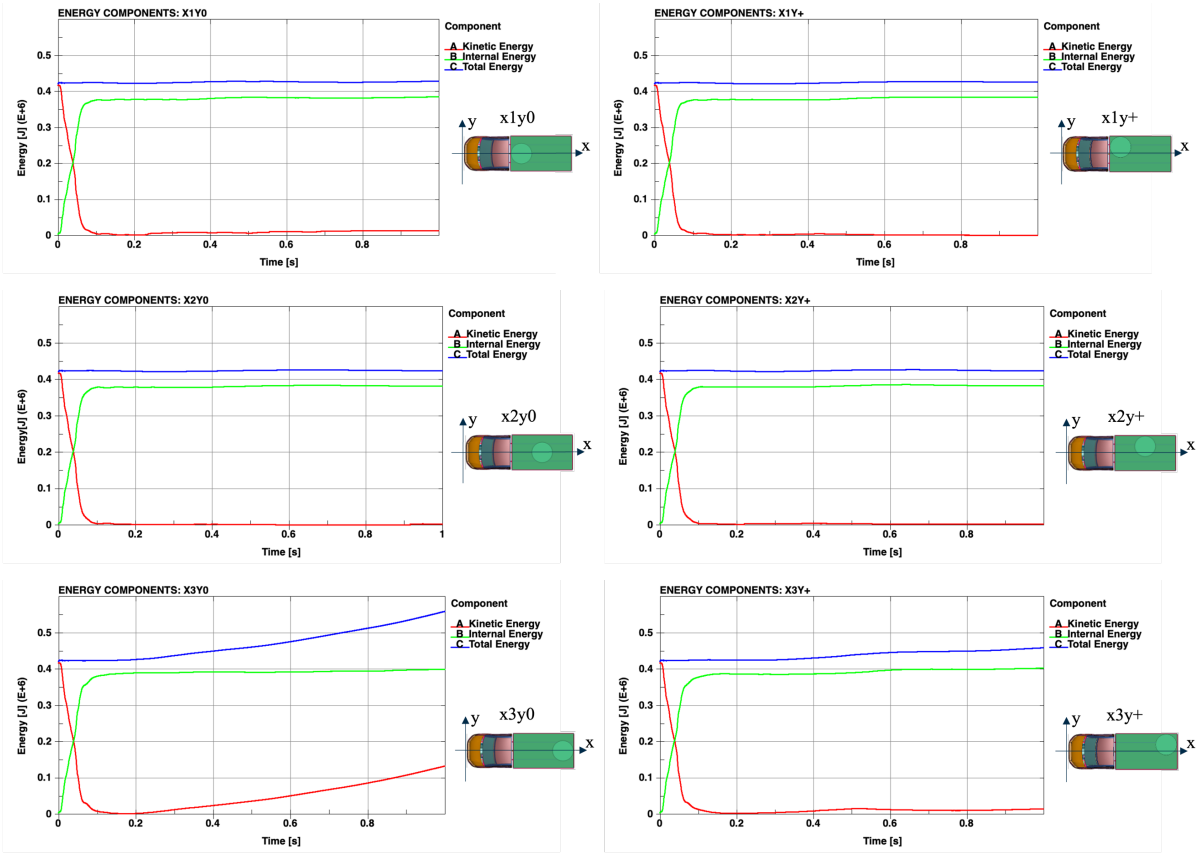

Figure 40. Cargo position influence: **e**nergy components

Contact force: X component

From the analysis of the contact forces (Figure 41) no evident differences are visible. Not only the peak force magnitude is similar maintaining the same cargo x coordinate and changing the y coordinate, but it is equivalent even moving the cargo along the flatbed. In addition, the part before the peak (from 0 to 0.05 s) is perfectly reproduced by all models.

The only difference is the time at which the force becomes equal to 0. In the models with the cargo in position x3, after the peak is reached, the force keeps decreasing and is equal to 0 at t=0.075 s, while in the other cases the force has a slight increase after that point because the vehicle is still in contact with the barrier until t=0.1 s.

The reason behind these differences is the position of the cargo: in the x3 cases it pulls the vehicle backward and separates it from the barrier prematurely, while in the models x1 and x2 the vehicle contacts the barrier for a longer time.

No other significant discrepancies are present, meaning that the contact force is poorly affected by the position of the cargo on the flatbed and the backward acceleration of the x3 models does not affect results.

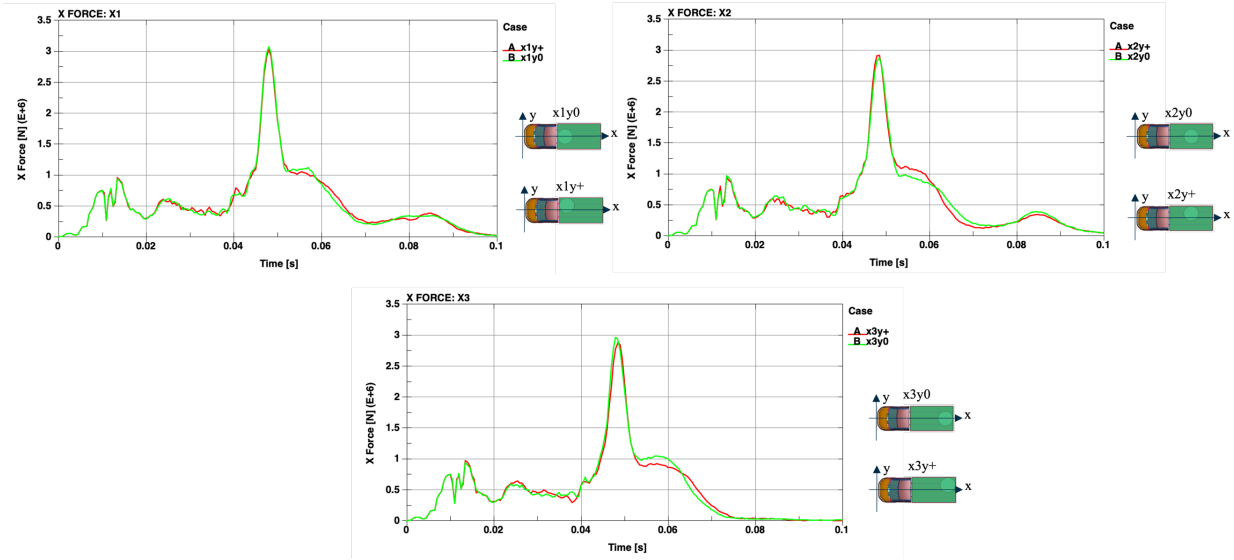

Figure 41. Cargo position influence: contact force

Momentum: X component

In Figure 42 it is possible to see the evolution of the momentum x-component over time. The curves are well overlapped in the x1 and x2 models even moving the cargo along y-direction.

The simulations with cargo in position x3, show a significant momentum increase after 0.1 s that anticipates the kinetic energy increase (which happens at t=0.2 s) shown in Figure 40. Again, the model with the mass decentered with respect to x-axis (x3y+) shows a minor momentum increase, even if still present and relevant. Model x3y0 momentum keeps increasing after the end of the simulation, meaning that the acceleration is not 0 and increases over time.

However, considering the initial part of the graph (from 0 to 0.1 s), when the vehicle is in contact with the barrier, curves of the x3 cases are very close to the others, meaning that the position of the cargo has little influence on the exchanged momentum with the barrier.

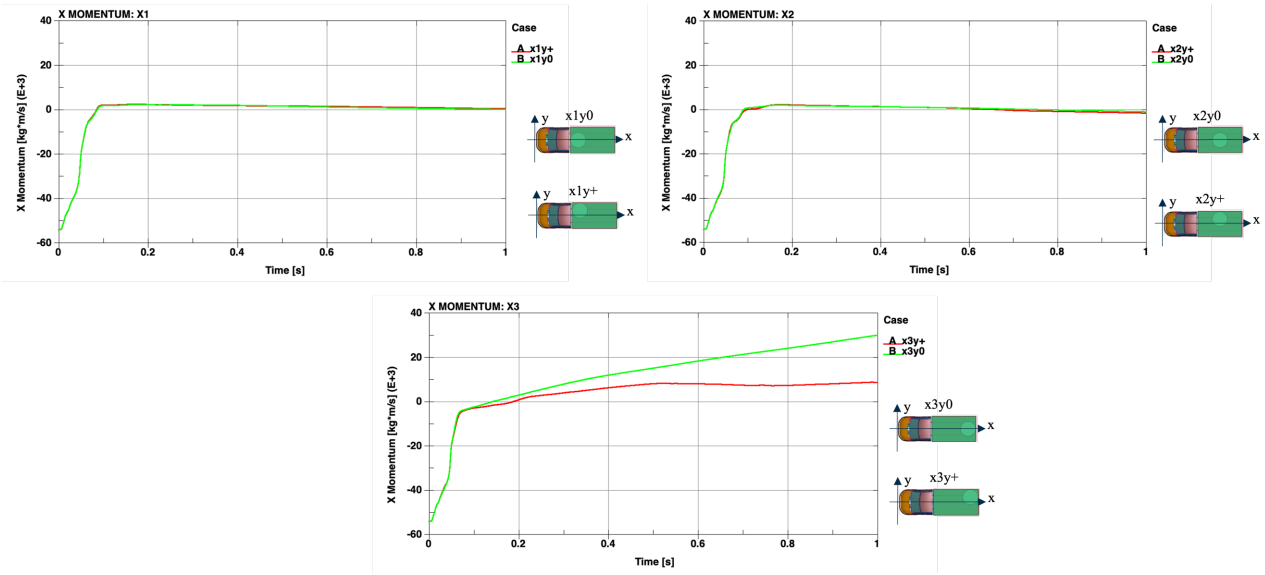

Figure 42. Cargo position influence: X momentum

In conclusion, previous results demonstrated that, contrary to the angle between barrier and vehicle, the position of the cargo has little influence on the results even moving the mass along y-direction. However, moving the component at the end of the flatbed (x3) showed a different and unusual behavior of the vehicle, which creates a different trend in the kinetic energy and momentum plots with respect to the other analyzed cases (x1 and x2), while the internal energy and the contact force are not affected by this phenomenon.

The reason is that after the impact, the cargo placed in this position bends the rear part of the flatbed, and accumulates energy on the longitudinal beams, like a spring. Then, the energy is released, and the vehicle is subjected to an acceleration in opposite direction. This acceleration is reflected by the increase seen in the kinetic energy and momentum plots, where the two curves increase after the end of the impact. In the model with the cargo in position x3y+ the phenomenon is less marked. It could be because the structure stores less energy during the impact, with the respect to the centered case (x3y0), due to the different deformation of the flatbed caused by the cargo.

On contrary, internal energy and contact force plots are not dependent on vehicle velocity and the phenomenon does not influence these results. Indeed, their plots are comparable to the other two cases with cargo near the cabin and cargo at the center of the flatbed (x1 and x2). This means that from the barrier point of view it is not a problem if the vehicle accelerates backward after the impact, because the transmitted forces and energies have been already exchanged.

However, it should be considered that:

- The constraint between cargo and flatbed floor is modeled as a rigid connection. In real cases, goods are normally fixed with stripes to avoid motion during travelling; however, in an impact like the one analyzed, it is more than probable that they would break.
- It is not common to place a 1-ton mass at the end of the flatbed. They are usually placed at the center or near the cabin to balance the vehicle center of gravity.

In the next section, the main tests performed on the x3y0 model to understand the causes behind and how to limit this phenomenon are discussed.

Backward acceleration testing

The present section is dedicated to the tests made on the model x3y0 in order to understand the causes behind the backward acceleration phenomenon. The simulation with non-centered cargo (x3y+) is not considered since the behavior is less present.

In the first part, a mass sensitivity analysis is made to find the point over which the acceleration arises. Then, several tests are made changing model parameters. Results are compared to the reference model presented in the previous section so that changes can be seen.

Mass sensitivity analysis

In the original x3y0 model, the mass of the cargo is equal to 1000 kg. According to official data, a FIAT Ducato [10] (one of the vehicles used as reference to create the N1 model) is capable of carrying good for a total mass which ranges between 1150 kg and 2075 kg, depending on the dimensions and characteristics of the model. Considering that the FEM model used during the analysis has a total length of 6200 mm, the maximum payload of the flatbed can be considered between 1500 kg and 1800 kg.

So, the mass used for the simulations is conform to the maximum load declared by the carmakers. However, it is important to understand if reducing the mass, it is possible to reduce or avoid the backward acceleration phenomenon.

To this aim, the cargo mass influence is analyzed gradually decreasing it from 1000 kg to 500 kg at intervals of 100 kg. In Figure 43 it is possible to see the results of the final instant of the animation (t = 1000 ms) for each case.

When the mass is between 500 kg and 700 kg, no acceleration arises after the impact. Indeed, in the shown frames the vehicles are settling and are not moving backward.

On contrary, starting from 800 kg the vehicle is still moving at the end of the simulation. The phenomenon is more evident in the two final cases (900 kg and 1000 kg) where the front axis is lift and the vehicle is getting further from the barrier.

Finally, it is possible to notice that the longitudinal beams have a lower deformation in the cases between 500 kg and 800 kg; while they are heavily deformed in the last two cases.

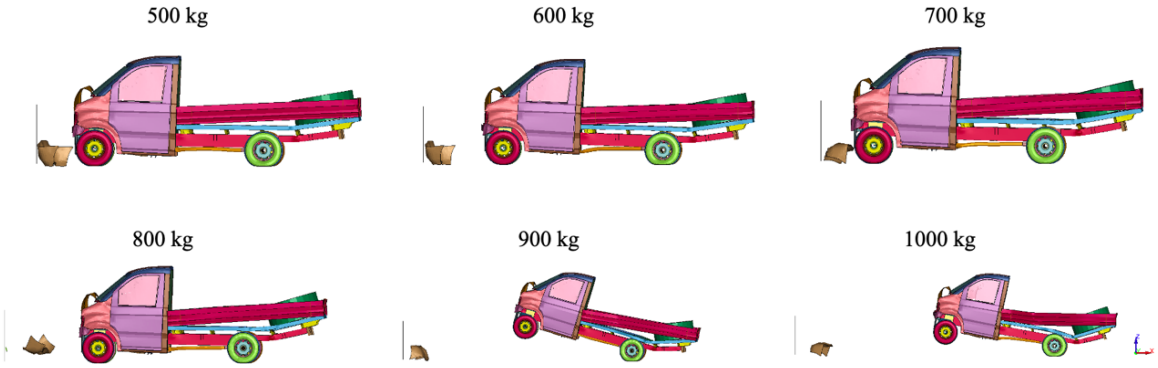

Figure 43. Backward acceleration testing: cargo mass sensitivity analysis

The analysis of the animation is confirmed by kinetic energy and momentum plots (Figure 44). The kinetic energy tends to 0 for the cases with cargo mass between 500 kg and 700 kg, while, starting from 800 kg, increasing the mass, the acceleration received by the vehicle increases as well.

The same considerations are valid for the momentum trend. However, it is possible to see that the 600 kg cargo (green curve) has a slight increase in momentum, even if the vehicle is stationary at the end of the simulation. Regarding the models with masses between 800 kg and 1000 kg, the momentum increases proportionally to the mass.

In the contact force plot, all curves are well overlapped, especially in the initial instants (0-0.05 s). The only difference between each model is the magnitude of the peak force, which decreases as the mass of the cargo is decreased.

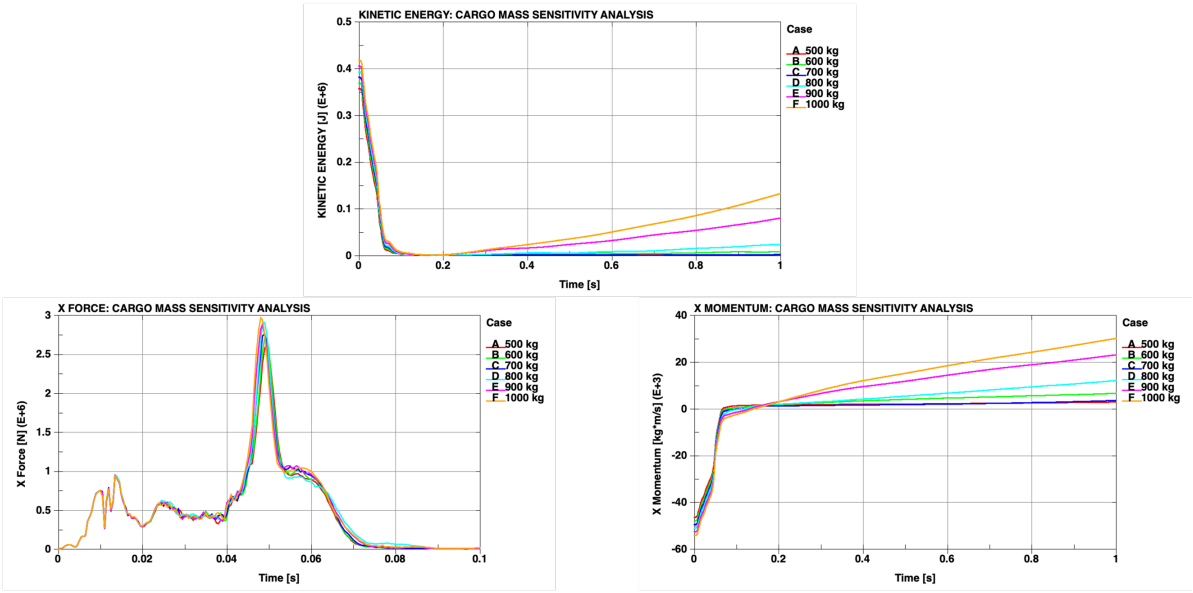

Figure 44. Backward acceleration testing: kinetic energy, contact force and momentum plots

Before changing other parameters of the model, the simulation time of the original model showed in the previous section (with the 1-ton mass) has been extended to 1.6 s to understand if the acceleration stops growing after a certain period. In Figure 45 it is possible to see the kinetic energy and the momentum at t=1.6 s. From the images, it is clear that the acceleration of the vehicle keeps increasing more and more over time.

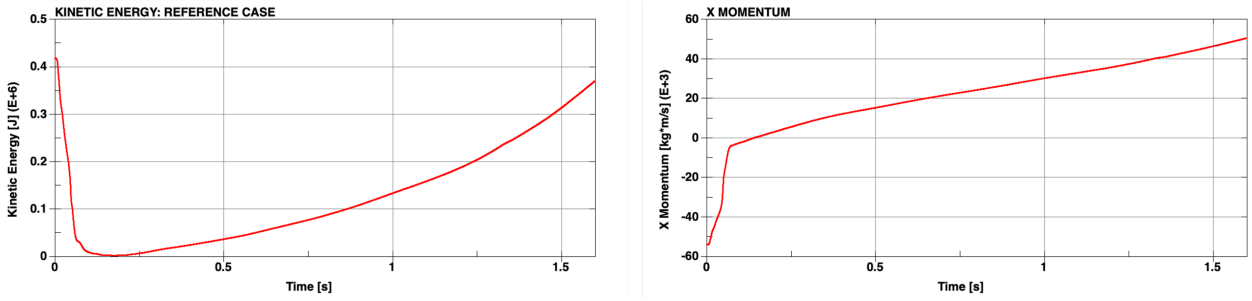

Figure 45. Backward acceleration testing: kinetic energy and momentum at t=1.6 s

Gravity influence

With the aim of understanding if the problem could be caused by the gravity applied on the model, the card responsible for the creation of the force is deleted from the model, and the simulation is run again. The last instant of the animation (Figure 46) shows that the vehicle front axis lifts even without gravity, and the vehicle moves back as in the case with the force applied.

Figure 46. Backward acceleration testing: model without gravity at t=1 s

Analyzing the energy components and the momentum plots (Figure 47) it is evident that the acceleration is even greater than the case with gravity normally applied on the model because both kinetic energy and a momentum reach higher values at the end of the simulation.

On contrary, contact force is unaffected by the presence of gravity force.

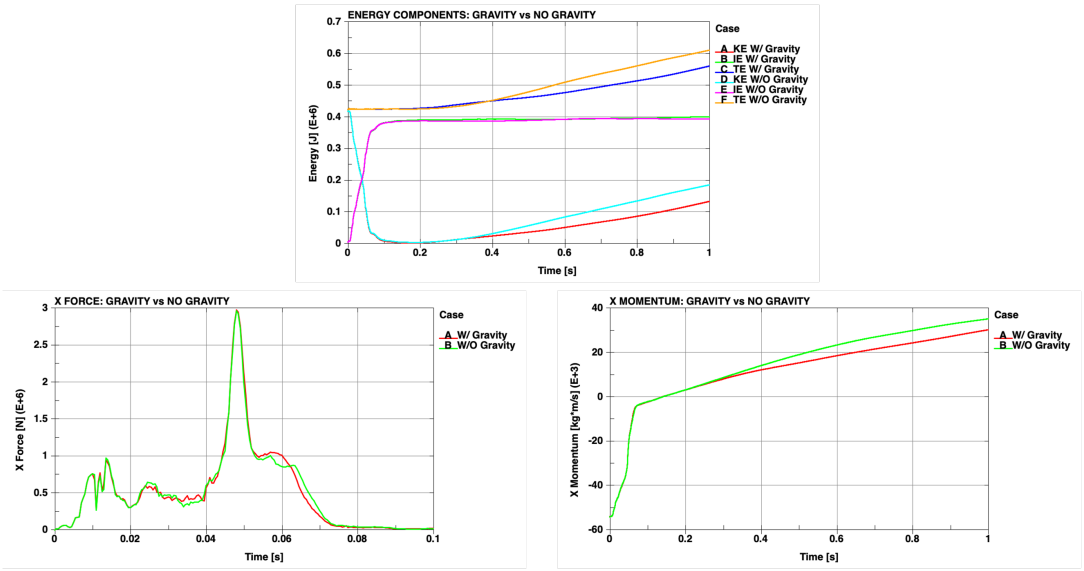

Figure 47. Backward acceleration testing: reference case vs no gravity plots

Rigid tires and suspensions

In the present test, the material of the tires is changed to rigid (from elastic) and the suspension stiffness is set to a value high enough to ensure a rigid behavior (10 kN/mm). The aim is to reduce the rotation of the cargo around the rear axis and to understand the effect of the suspension system. In Figure 48 it is possible to see that the vehicle is very far from the barrier because of the acceleration which arises after the impact. In addition, the vehicle is subject to a yaw rotation

which makes the N1 model turn left while going backward, as can be seen from picture. The reason of this motion is that during the impact both front tires are turned to the left (Figure 49). As a consequence, when the vehicle gains the acceleration, they direct the vehicle in this direction.

Figure 48. Backward acceleration testing: model with rigid tires and suspensions at t=1 s

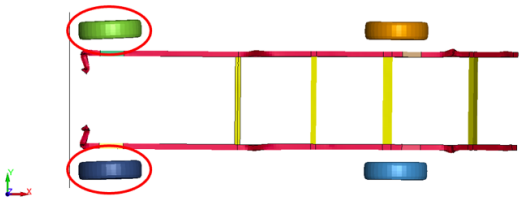

Figure 49. Backward acceleration testing: inclination of the rigid tires at t=0.18 s

The kinetic energy comparison with the reference case (Figure 50) shows a net increase in the model with rigid tires caused by a higher acceleration gained by the vehicle. The momentum plot presents the same trend, being higher than the reference case.

The contact force is not affected by the different material used for the tires and by the stiff suspensions adopted.

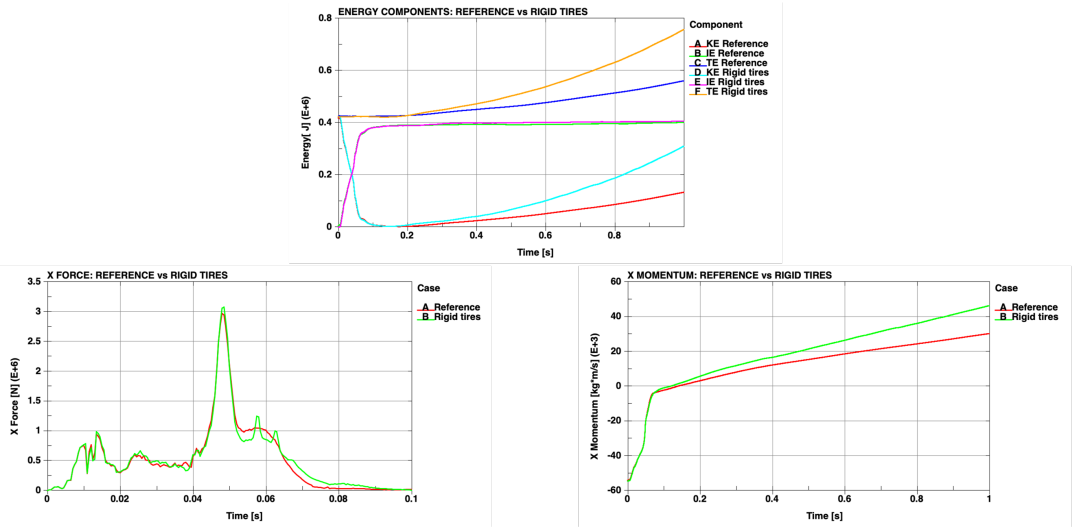

Figure 50. Backward acceleration testing: reference case vs rigid tires and suspensions plots

Rigid skin

The original constraint present between the cargo and the flatbed is of rigid type. With the aim of testing the contact algorithm between cargo and flatbed the relationship between these two components is changed. The cargo is surrounded by a skin of rigid elements with which has a traditional contact relationship and it's able to move inside this component. The skin is then rigidly constrained with the flatbed. An overview of the model and a section of the cargo surrounded by the skin can be seen in Figure 51. A gap of around 1 mm is present between the two parts.

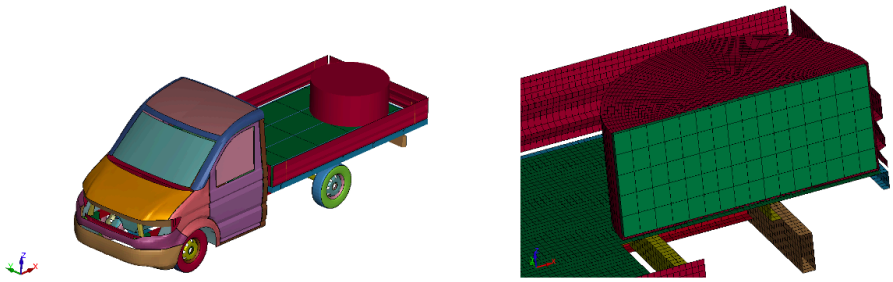

Figure 51. Backward acceleration testing: cargo rigid skin

The animation shows a behavior analogue to the case without skin (Figure 52). During the impact the cargo moves inside the available space; however, the two parts are rigid, and the inertia of the cargo is totally transmitted to the flatbed by the skin.

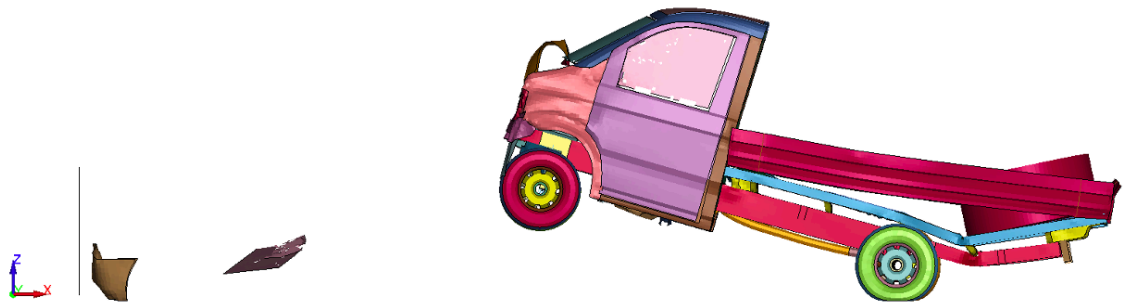

Figure 52. Backward acceleration testing: cargo with rigid skin at t=1 s

Very little changes can be seen in the kinetic energy and momentum plot (Figure 53) because in the end, a rigid connection is still present with the flatbed.

Contact force plots are, again, well overlapped.

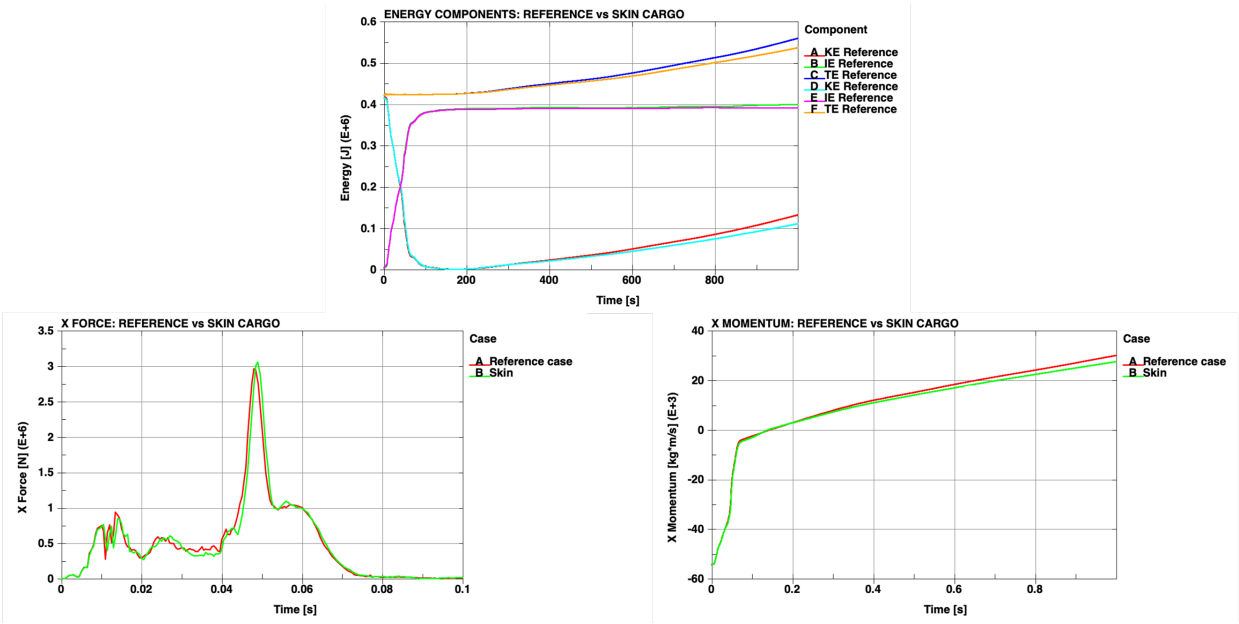

Figure 53. Backward acceleration testing: cargo without skin vs cargo with skin plots

Other types of material (plastic and elastic) have been tested to model the cargo skin; however, the deformation of the flatbed is always the same as well as kinetic energy and momentum plots.

Rigid frame

In this section, it is analyzed the influence of the longitudinal beams to understand if the accumulated internal energy during the impact triggers the phenomenon.

To this aim, half of the longitudinal beams are modeled with a rigid material. In particular, the front part is left untouched, so that it can normally deforms against the barrier, while the portion which deforms more (from the center and finishing to the rear end), is modeled with a rigid material (Figure 54). The very last column of elements is left as plastic material since rigid connections are applied to these nodes and they can be only linked to non-rigid elements.

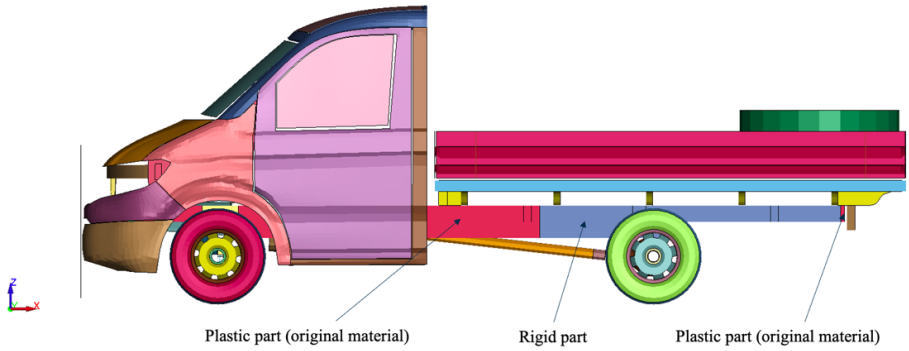

Figure 54. Backward acceleration testing: model with rigid longitudinal beams

Analyzing the animation at the last instant (Figure 55), it is possible to notice that the vehicle is not far from the barrier as in the other cases because there is no acceleration gain after the impact. The front part deforms in accordance with the models seen in the previous section (x1 and x2). In the rear part, being the longitudinal beams rigid, they cannot deform. As a consequence, the flatbed deforms absorbing the energy of the cargo.

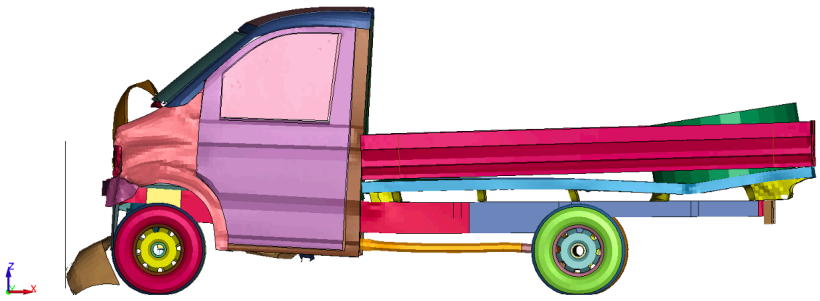

Figure 55. Backward acceleration testing: model with rigid frame at t=1 s

Kinetic energy and momentum plots (Figure 56) confirm that there is no acceleration gain after the impact of the vehicle. In both cases, the curve remains constantly equal to 0 until the end of the simulation.

The contact force is not affected by the adoption of a rigid portion of the longitudinal beams.

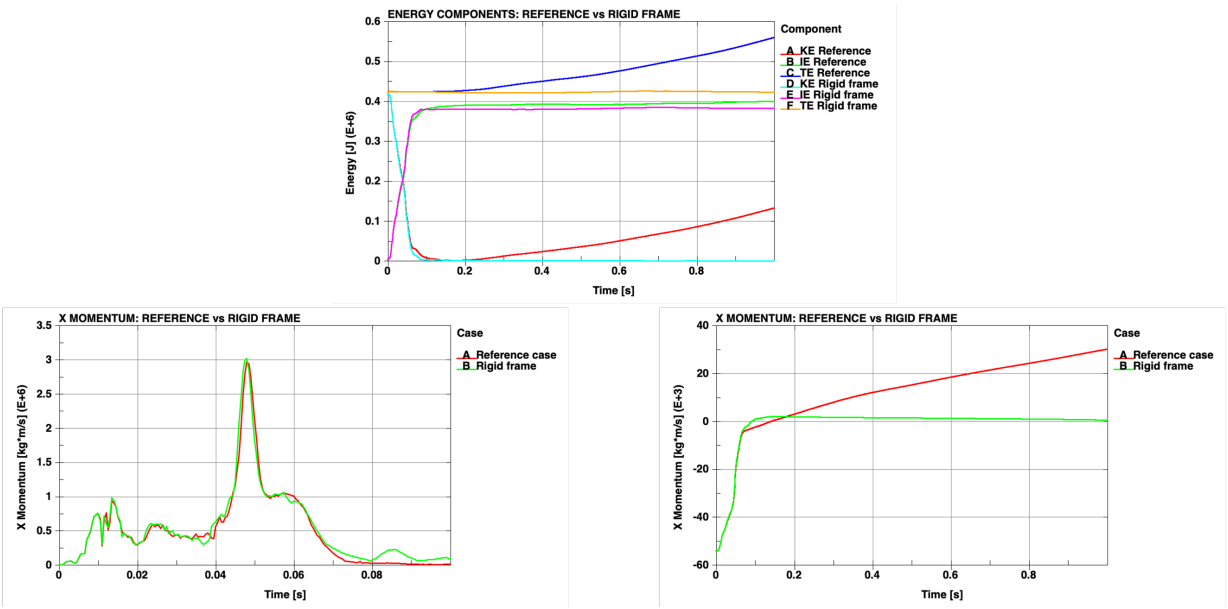

Figure 56. Backward acceleration testing: reference model vs rigid frame plots

Interestingly, the internal energy of the two cases is almost the same, even if in the "rigid frame" case, the overall deformation of the vehicle is different. In particular, it is possible to compare the internal energy and the kinetic energy of the same portion of longitudinal beams between the reference case and the "rigid frame" model, in order to understand the differences. Figure 57 shows that, while the kinetic energy is the same in the two cases, when a rigid material is used to model the longitudinal beams, the internal energy absorbed by the part is equal to 0. On contrary, if a plastic material is used, as in the reference case, the components deform and absorb internal energy.

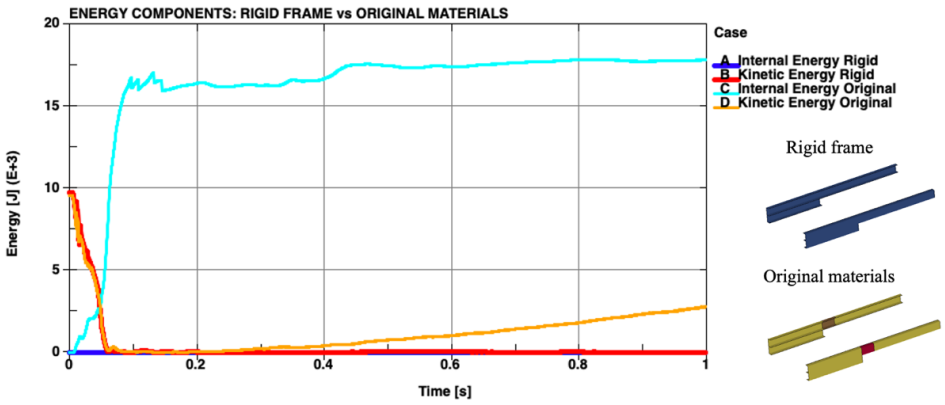

Figure 57. Backward acceleration testing: reference case vs rigid frame. Energies of the changed part

This means that the internal energy, which is not absorbed by the rigid longitudinal beams, is absorbed by other parts, so that in the end the total internal energy of the vehicle is close to the case with plastic longitudinal beams.

In Table 3, it is possible to see the comparison of the internal energy absorbed by each single component of the vehicle between the reference case (with fully plastic longitudinal beams) and the "rigid frame" case. In the table, only the components with the highest influence are shown. Overall, the internal energy which is not absorbed by the rigid portion of the longitudinal beams, is distributed among the front components; in particular, the front part of the longitudinal beams, the hood and the wheel arch absorb more energy with respect to the reference model.

The biggest change in internal energy is exhibited by the flatbed crossbar, which is the set of crossbeams connecting the flatbed to the longitudinal beams. In the reference model, they have little deformation because they transmit the weight of the cargo to the longitudinal beams.

Component	Internal energy Rigid frame (J)	Internal Energy Plastic frame (J)	% of change of the rigid frame wrt to plastic
Longitudinal beams	6.96e+4	6.42e+4	+8.4%
Frame crush zone	5.98e+4	6.10e+4	-1.97%
Wheel arch	2.71e+4	2.40e+4	+12.9%
Flatbed crossbar	2.26e+4	1.51e+4	+49.7%
Front fascia bottom	1.70e+4	1.84e+4	-7.6%
Front cross member	1.67e+4	1.67e+4	0%
Front inside panel	1.44e+4	1.37e+4	+5.1%
Hood	1.12e+4	1.05e+4	+6.7%
Driving shaft	1.11e+4	1.15e+4	-3.5%
Front bumper absorbing element	9.92e+3	1.21e+4	-18.0%

Table 3. Backward acceleration testing: components internal energy

On contrary, in the tested model, they are crushed by the mass on the rigid beams, which are undeformed.

The total internal energy of the components of the "rigid frame" model shown in Table 3 is equal to 25.94e+4 J, while the total internal energy of the same components from the reference model is equal to 24.72e+4 J. So, the energy absorbed by the components in the "rigid frame" case is slightly higher than in the reference case. However, there are lots of components with lower order of magnitude which balance the global internal energy of the whole vehicle.

In general, it is possible to affirm that: the components located in the front part of the vehicle absorb more internal energy when a rigid material is used to model half of the longitudinal beams; while the parts located in the rear part of the vehicle absorb less internal energy due to the lower deformation imposed by the rigid frame.

In conclusion, the presented test showed the importance of the longitudinal beams in hindering the acceleration of the vehicle after the impact against the barrier. Indeed, limiting the deformation and the energy absorbed by these components, completely avoid the phenomenon, while maintaining the same level of force transmitted to the barrier.

Lengthened vehicle

In this section the total length of the vehicle is changed, as well as the position of the cargo, in order to create a different deformation of the longitudinal beams. Starting from the reference model (with all the original materials and components), the length of the vehicle to the maximum length that could be set in the parameter file, as shown in Figure 58. This change does not affect the dimensions of the front part but impacts only on the total length of the flatbed. For this reason, the cargo is moved from 5550 mm to 5920 mm so that it is always at the end of the vehicle.

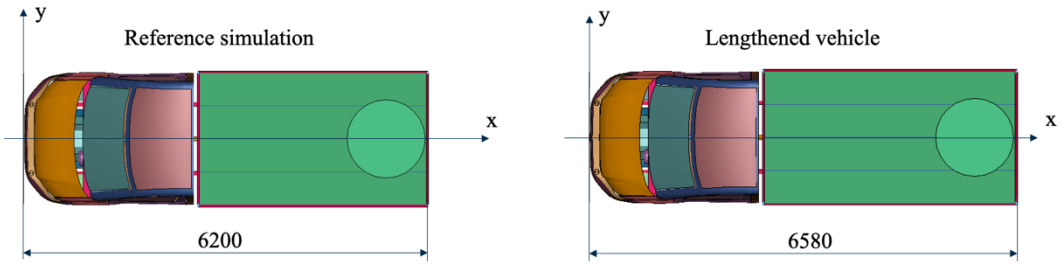

Figure 58. Backward acceleration testing: lengthened vehicle setup

Figure 59 represents the last instant of the simulation with lengthened vehicle. It is possible to notice that the vehicle is close to the barrier at the end of the simulation because no acceleration

is gained after the impact. The deformation of the longitudinal beams is lower with respect to the reference case, while the deformation of the flatbed is very similar.

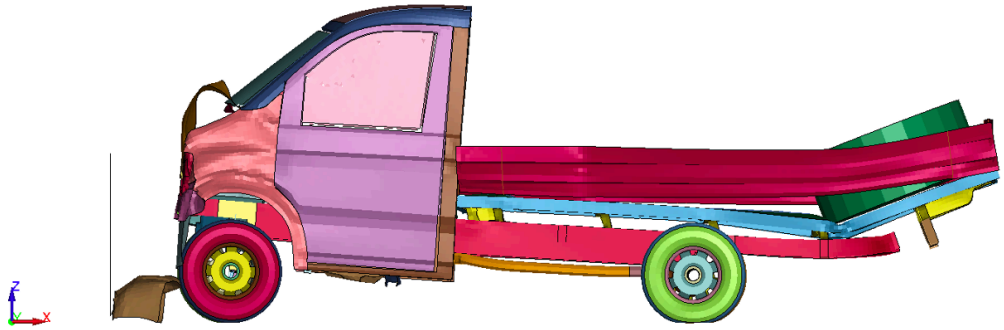

Figure 59. Backward acceleration testing: lengthened vehicle at t=1 s

The comparison of the kinetic energy and momentum plots of the reference model with the examined case (Figure 60), confirms that there is no gained acceleration after the vehicle impacts the barrier. In addition, the internal energy absorbed by the two models is almost identical, as well as the transmitted force.

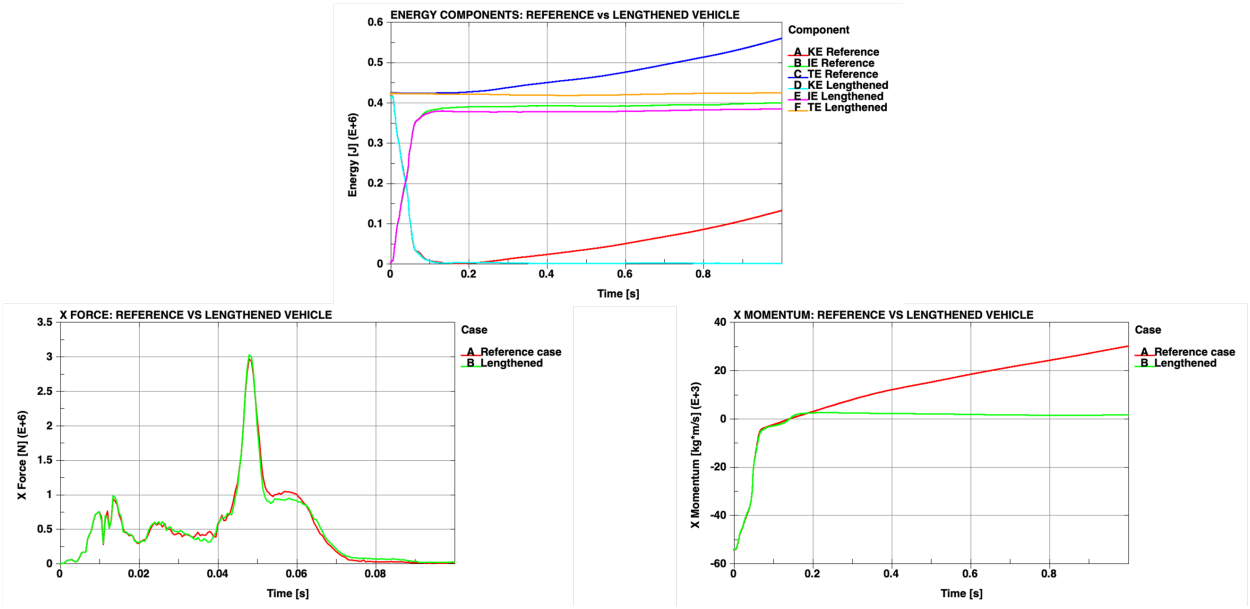

Figure 60. Backward acceleration testing: reference vs lengthened vehicle plots

In conclusion, the presented tests demonstrated the main role of the longitudinal beams in the creation of the acceleration gained by the vehicle after the impact. The deformation and the energy absorbed by these two components create a spring-effect, which can be avoided in different ways:

reducing the mass of the cargo, stiffening the portion of longitudinal beams placed under the cargo (which is the most deformed part), or increasing the total length of the vehicle.

However, it should be considered that the transmitted force is equivalent in all analyzed cases, also the ones without backward acceleration. It means that for barrier testing, the input forces and energies are correctly received from the vehicle.

In addition, it is not common to place a 1-ton mass at the end of the flatbed. They are generally placed in central position or near the cabin to balance the vehicle while travelling.

Future tests could be made on the constraint type between flatbed and cargo, to create a fixing method with rupture limit to allow the cargo to dissipate part of its energy instead of fully transmitting it to the flatbed (and consequently to the longitudinal beams).

Chapter 3

Bollard impact

Bollards are one of the most adopted solutions for the protection of public spaces. They can have different shapes, ornamental features, and they can movable. These devices are normally seen on sidewalks, squares and at protection of buildings. The main advantage with respect to a wall, is that they can let people pass through while limiting the access to vehicles. This is done by setting the space between consecutive bollards.

In this chapter, the impact between the N1 model and a rigid bollard is analysed. The whole simulation is set to reproduce an experimental test [11] of which only the video is publicly available. Images of the experimental test are elaborated on the software Tracker by OSP [12] to extrapolate the kinematic properties and the deformations. Then, results are compared with the plots obtained from the accelerometers placed in the N1 model.

First, the dimensions of the bollard are taken from official constructor data (presented in the video). The model of bollard used in the test is the: ALE F16-100-C50 [13]. The device is modelled in LS-PrePost (Figure 61) with rigid shell elements and the same material used to model the planar barrier of the previous chapters (Steel).

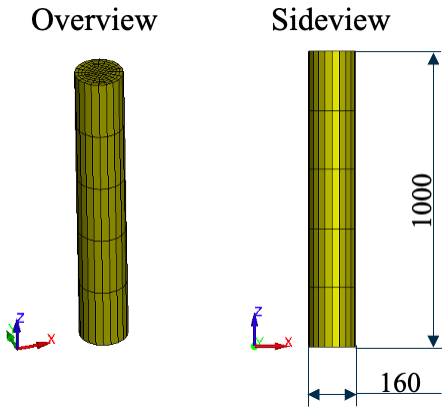

Figure 61. Bollard geometry

Then, the dimensions of the vehicle are extracted from two frames of the video in which the vehicle is stationary (Figure 59). In particular, the wheelbase, the total length and the wheel track

are measured to be set in the parameter.k file of the FEM model. To calibrate the ruler, the program must know which is the scale of the image. For the purpose, a calibration tool consisting of an adjustable stick, is placed on the height of the bollard, because it's the only element with known dimensions. Then, the ruler can be used to measure the needed dimensions with the correct scale.

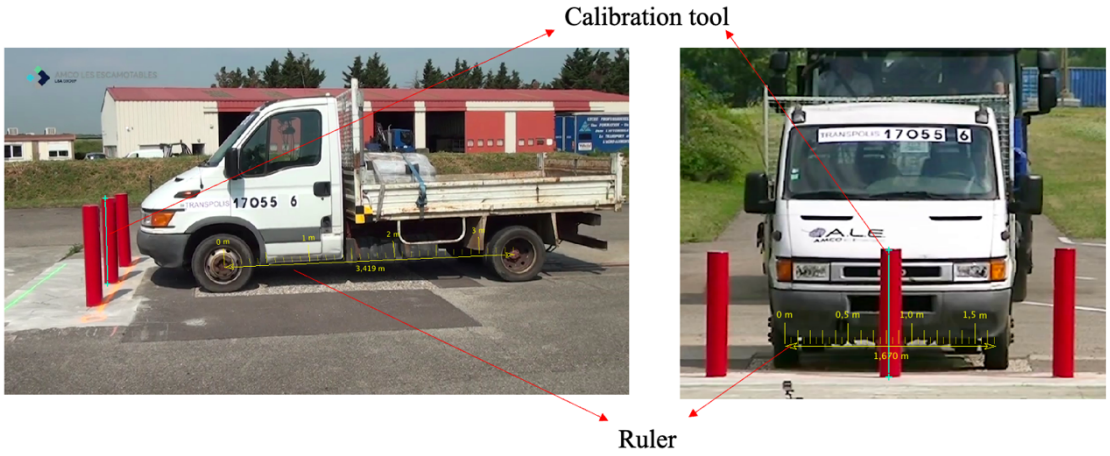

Figure 62. Bollard impact: experimental test reverse engineering

In addition to the dimensions of the vehicle, the total mass of the model (vehicle + cargo) and the impact velocity are declared in the experimental test video, so they are easily set in the virtual model. The final setup of the model is presented in Table 4.

Parameter	Value
Impact velocity (km/h)	48
Barrier-Vehicle friction coefficient	0.5
Total mass: cargo + vehicle (kg)	3500
Vehicle length (mm)	5820
Wheelbase (mm)	3420
Wheel track (mm)	1670

Table 4. Bollard impact: vehicle setup

Once all dimensions and parameters are set in the FEM model to be as close as possible to the one of the real vehicle, the bollard is placed in central position with respect to the front part of the N1 model, as shown in Figure 63, and the simulation is run with a duration of 1000 ms.

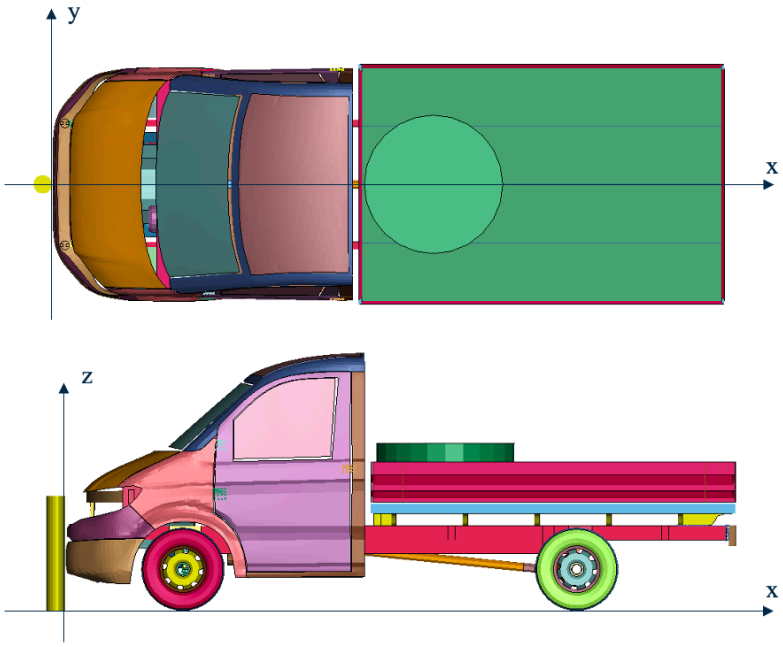

Figure 63. Bollard-vehicle setup

Comparing the side view of the impact of the virtual model with the side view of the video of the experimental test (Figure 64), it is possible to see a very good correlation between the two images. The deformation of the hood of the real vehicle is well reproduced by the FEM model, as well as the rupture of the transmission and the deformation of the flatbed.

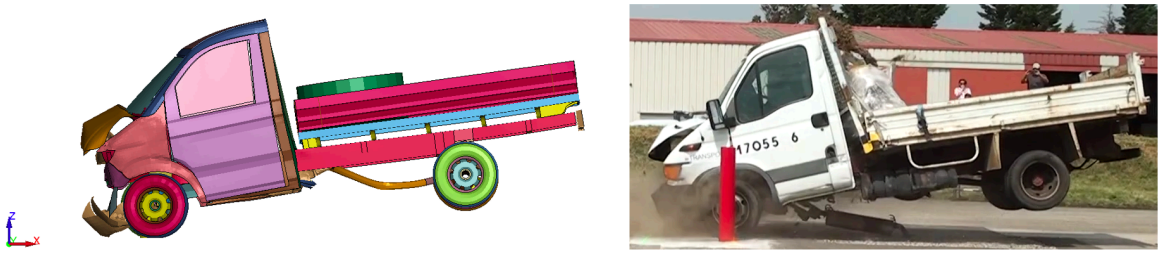

Figure 64. Bollard impact: side view comparison

In Figure 65 the front view comparison between the experimental test and virtual test is shown. The overall deformation of the front elements is very close in the two cases. In particular, the hood is subjected to an indentation caused by the top part of the bollard, while the front bumper impacts the central part of the barrier. This component is the most deformed in this type of impact, and bend around the bollard as the simulation proceeds.

Figure 65. Bollard impact: front view

Finally, a 45-degree view (Figure 66) provides a better view of both the front and lateral parts. The two images show a good correlation in the deformation and in the crash kinematic of the two cases, considering that even if the N1 model has been set with the dimensions of the experimental test, it is a generic vehicle, so it doesn't have the very same components and geometries of the real vehicle.

Figure 66. Bollard impact: 45° view

In order to deepen the analysis between the two models, a comparison of the kinematic results and of the deformations is done. Before adopting the use of the software Tracker on the experimental test video, the procedure is validated using the animation of the virtual model and comparing the results from LSPP.

Tracker procedure validation

All analysis procedure adopted to extract data from the experimental test video have been validated comparing the results from the virtual simulation on LS-PrePost, and the video of the animation of the same simulation processed on Tracker.

The first validation is the analysis of the deceleration. Three points are selected from the N1 model (Figure 67). Each of these points have been marked on Tracker to follow its evolution over time and obtain the plot of the velocity.

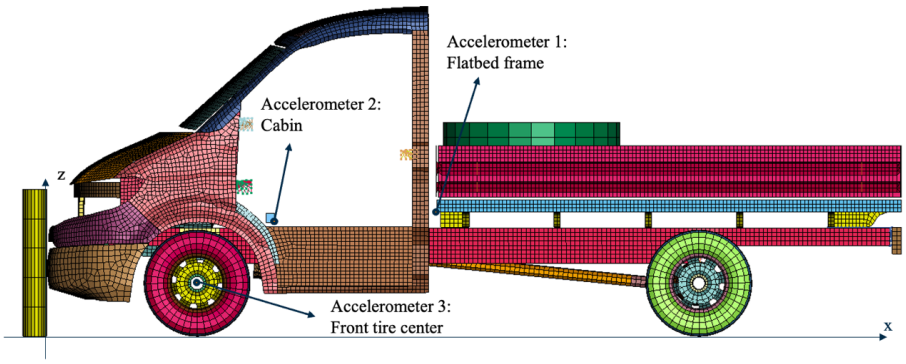

Figure 67. Bollard impact: accelerometers for deceleration computation

In Figure 68 it is possible to see the comparison between the resultant velocity plot of the point shown in Figure 67. Each graph compares the curve obtained from the accelerometer of the N1 model in LS-PrePost (red), and the curve obtained marking the same point in the animation video of the FEM model in Tracker (green).

A perfect overlapping between the two curves is present, meaning that the procedure is validated and can be adopted for the computation of the deceleration of the experimental test.

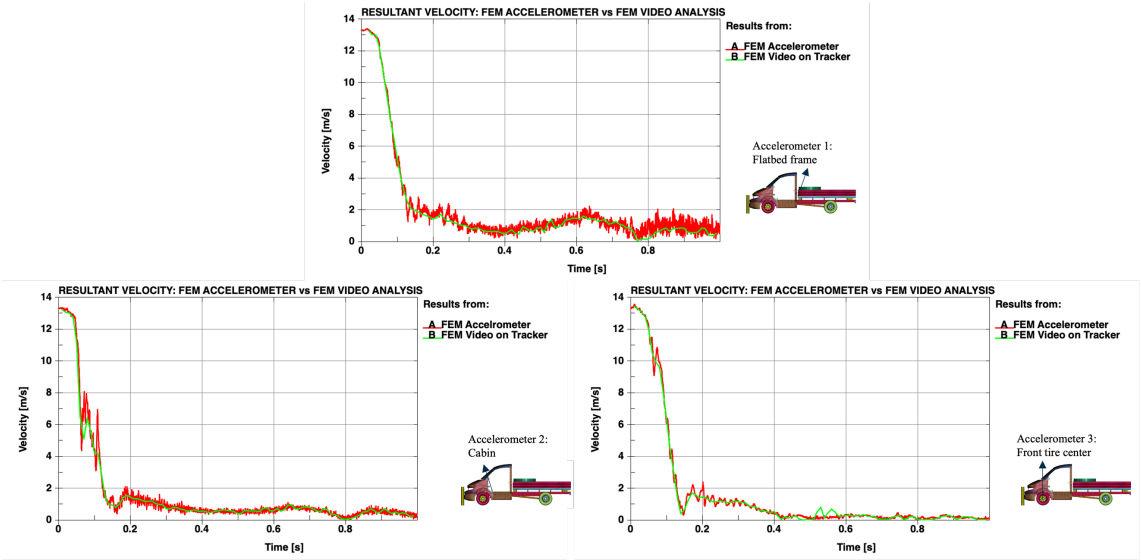

Figure 68. Bollard impact: deceleration validation

The second validation procedure concerns the deformation of the front part. To measure the penetration of the bollard inside the front part of the vehicle, the reference system z-axis is placed

along the bollard right face. Marking the point corresponding to Accelerometer 1, it is possible to determine its x coordinate displacement over time. As the vehicle moves, the point gets closer to the z-axis (which is the bollard right face), and so it corresponds to the penetration of the bollard inside the front part of the vehicle. In Figure 69 it is possible to see the comparison between the accelerometer x-coordinate change in LS-PrePost (red curve) and the evolution of the same point marked on the video of the virtual model on Tracker.

A perfect overlap of the two curves can be seen in the plot, meaning that the procedure is validated and can be used on the experimental test video. However, the presented method has an acceptable accuracy up to the maximum deformation (at t=0.1 s). Over that point, the method is not able to catch the residual deformations of the structure, because the vehicle moves back and so the marked point gets further from the z-axis. This is why there is a big reduction of deformation after the peak point.

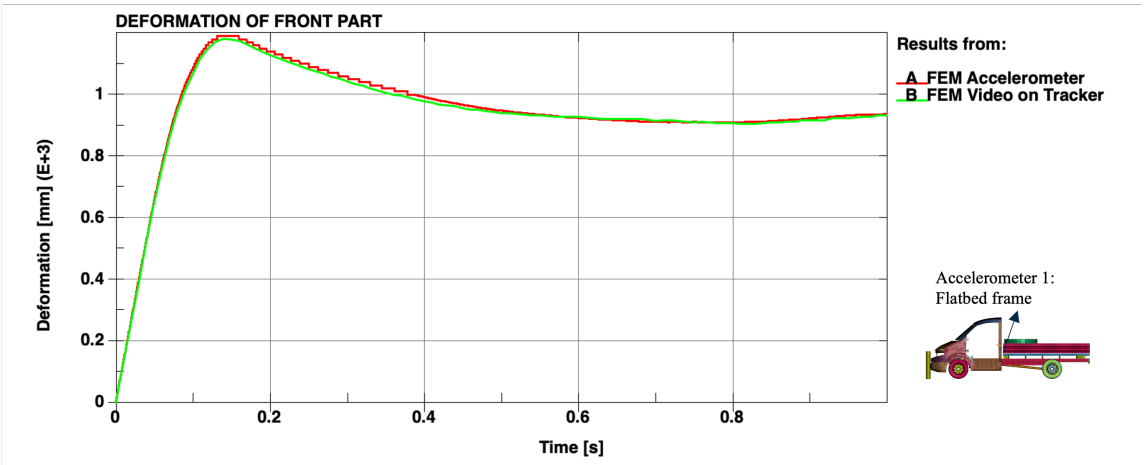

Figure 69. Bollard impact: deformations validation

With the aim of comparing the lift of the rear part of the vehicle during the impact, two points are marked on Tracker (Figure 70): one on the flatbed end, and the other on the rear tire center. Since in the real experiment it is not possible to determine the initial z-coordinate of the points with precision, the x axis is placed at different heights for the two cases. It is aligned so that it passes through the marker position at the first instant. In this way, any vertical movement of the marker during the simulation corresponds to a change with respect to its initial position.

In Figure 71 it is possible to see the results of the comparison. The data from the accelerometer in LS-PrePost (red curve) are perfectly overlapped to the data from the marked point in Tracker (green curve). So, the procedure is validated and can be used to compare the vertical motion of the virtual model with the vertical motion of the vehicle in the experimental test.

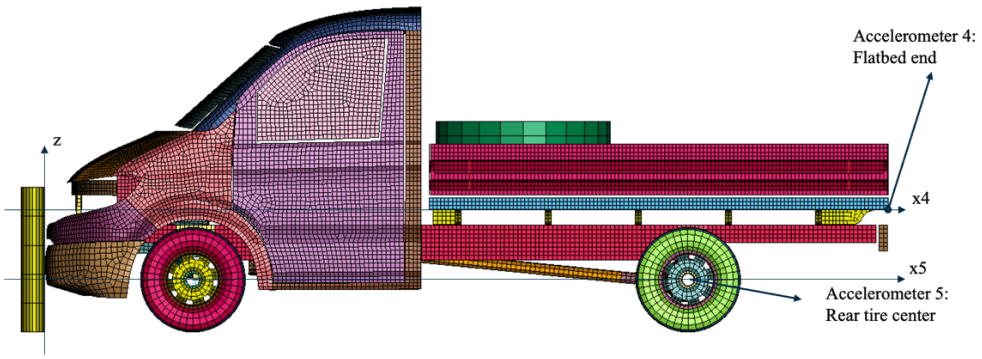

Figure 70. Bollard impact: accelerometers for rear lift computation

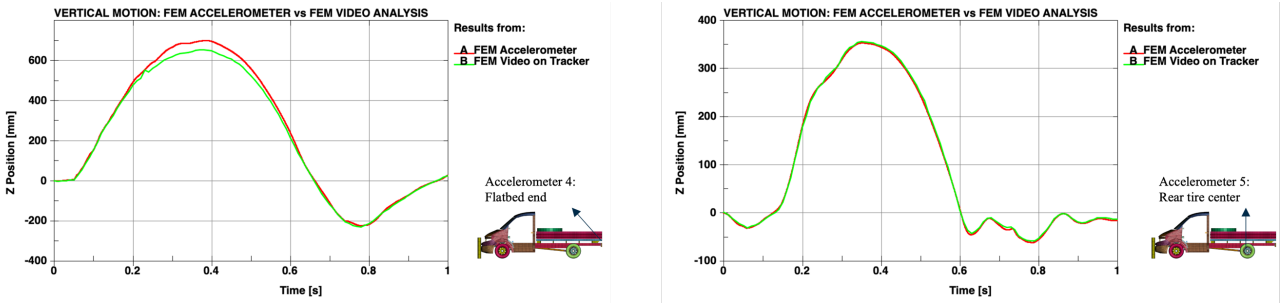

Figure 71. Bollard impact: vertical motion validation

Finally, the last comparison concerns the angle created by the vehicle during the impact with the horizontal. To this aim, two points are taken from the longitudinal beams (Figure 72). In LS-PrePost, it is possible to measure the angle created by a line connecting these two points with respect to the horizontal using an implemented tool. On tracker, a reference system is placed in correspondence of Point 2, while a marker is present in correspondence of Point 1. In this way, as the vehicle moves, the reference system will translate following Point 2 (without rotations), and the angle created by the marked point is measured as rotation around that system.

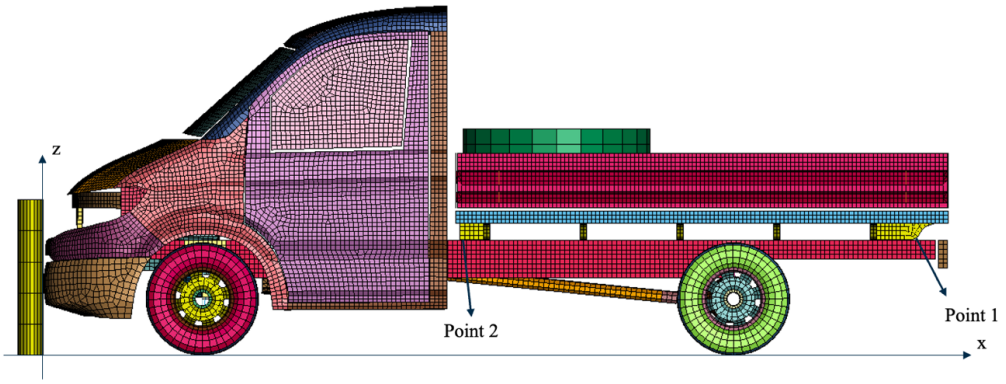

Figure 72. Bollard impact: points for angle of inclination computation

Results shown in Figure 73 demonstrate the accuracy of the procedure, which can be adopted to extract data from the experimental test video.

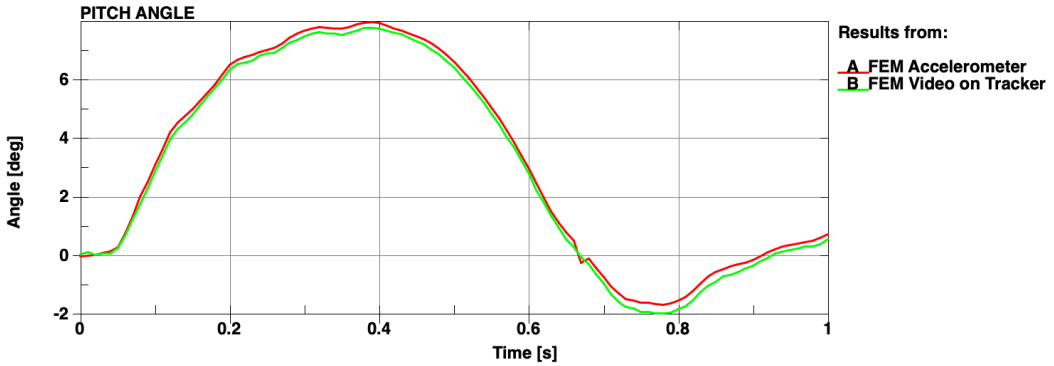

Figure 73. Bollard impact: vehicle angle measure validation

In the end, all procedures for extracting data from the experimental test video by means of the software Tracker have been validated. These techniques will be used in the following section.

Experimental test - N1 model comparison

For all the presented analysis in this section, the experimental test is processed on Tracker to extract the necessary information. The accelerometer of the FEM model is placed in correspondence of the marker of the real vehicle. For what the N1 model is concerned, data are obtained from LS-PrePost, extracting the necessary information from the accelerometers.

The first analysis is the comparison of the decelerations. The setup of the experimental test video on Tracker and the accelerometer used in LS-PrePost are shown in Figure 74.

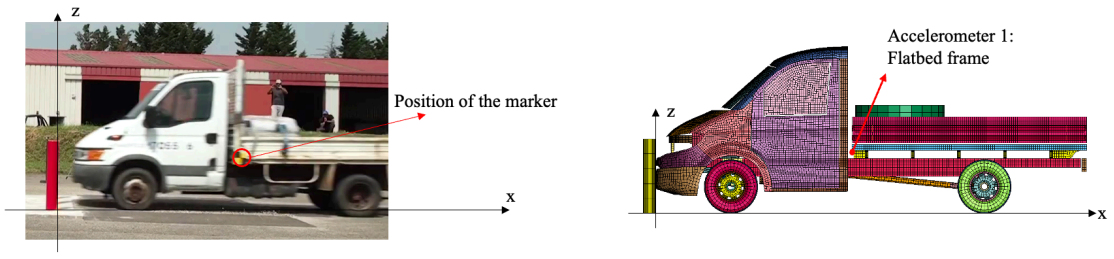

Figure 74. Bollard impact: deceleration comparison setup

In Figure 75 it is possible to see the resultant velocity of the data coming from Tracker (for the experimental test) and from LS-PrePost (for the virtual model). Since in the experimental test video the last frame before the impact has a certain gap from the bollard, while in the virtual model it is in contact with the bollard, a time shift is applied to the green curve to compensate

this difference and have more comparable results. This shift is applied to all curves presented in the following.

A very good relationship can be appreciated regarding the overall trend of the two curves. Not only the initial deceleration (from 0 s to 0.15 s) is close, but also the instants after the vehicle has stopped are well overlapped.

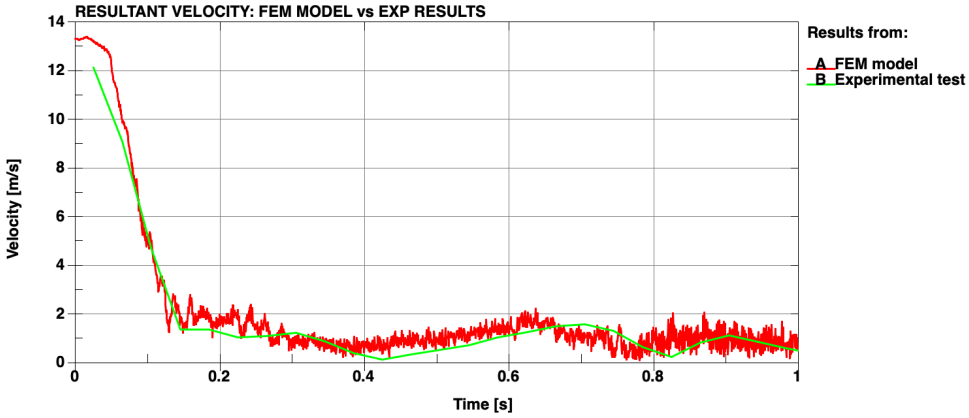

Figure 75 Bollard impact: deceleration plot

Using the same setup shown in Figure 74, it is possible to compute the penetration of the bollard inside the front part of the vehicle. Figure 76 shows the results obtained from the experimental test video analysis on Tracker (green curve) and from the accelerometer of the virtual model on LS-PrePost (red curve). A good correlation is seen up to the maximum deformation, which occurs at the same time and has a difference lower than 10 %. More evident differences are present after the maximum, due to the different motion of the vehicle after the impact. The method adopted to compute the deformation is reliable only up to the maximum deformation. Residual deformations cannot be obtained.

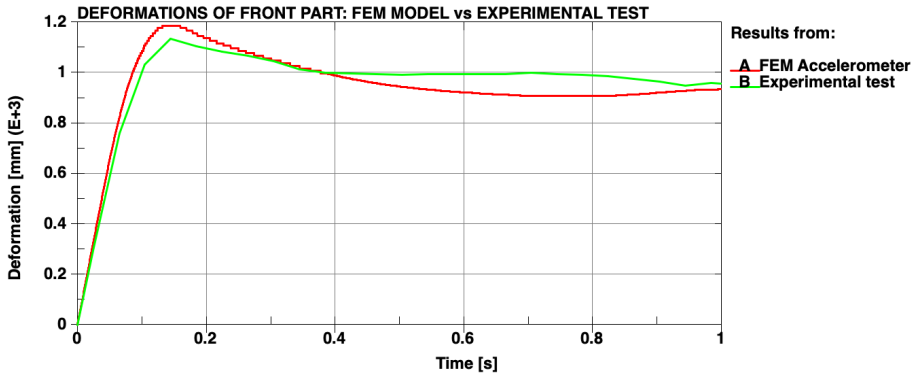

Figure 76. Bollard impact: front deformations plot

In order to deepen the analysis of the kinematic of the vehicle during the impact, the vertical motion of the rear part of the two models is compared. Two markers are placed on the experimental test video on Tracker (Figure 77): one on the flatbed end (Marker 2) and one on the rear tire center (Marker 3). Since the flatbed end is not visible from the last frame before the impact, data extraction is delayed with respect to Marker 3 and starts from t=0.08 s from the beginning of the simulation. Accelerometers are placed in correspondence of the same point on the virtual model.

Since the two models (real and virtual) have different initial heights for the two markers, the reference system of the experimental test video is placed with the x axis passing through the initial position of each marker. In this way, the initial value of the vertical displacement is equal to 0 as for the data of the accelerometers in LS-PrePost.

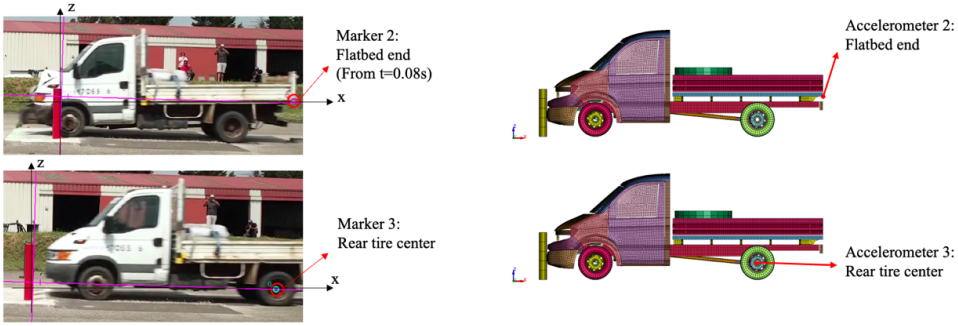

Figure 77. Bollard impact: vertical motion comparison setup

The comparison of the vertical motion of the vehicles (Figure 78) shows a greater correlation for what the rear part of the flatbed is concerned. The two curves follow the same path and reach almost the same displacement at the same time. Bigger differences are present after the top height is reached. About the vertical motion of the rear axle, the maximum vertical displacement is greater in the real case with respect to the virtual model. The reason could be a different tuning of the suspension systems.

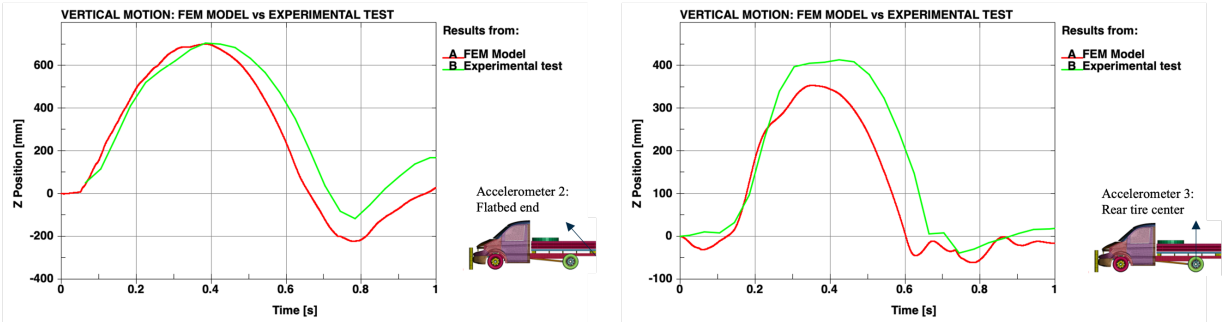

Figure 78. Bollard impact: vertical motion plots

The final analysis is the comparison of the angle of inclination created by the rear part of the vehicle when it impacts the bollard and the rear part lifts.

In Tracker, a reference frame which moves with a marked point is used in combination with Marker 2 (Figure 79). Again, the rear part of flatbed is visible from t=0.08 s. The reference system x-axis passes through Marker 2 at the initial instant in order to have a 0-degree angle at the beginning.

Regarding the FEM model, the angle formed by the line connecting Point 1 and Point 2 is computed with a tool implemented in LS-PrePost.

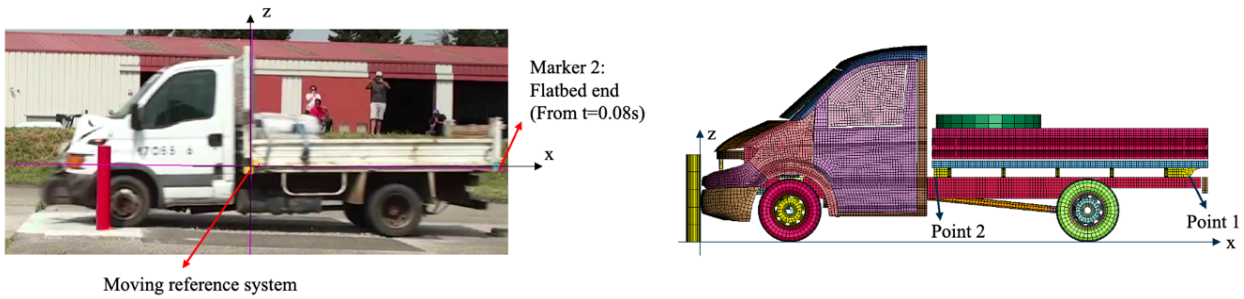

Figure 79. Bollard impact: angle of inclination comparison setup

Small differences can be seen in the results of the two models (Figure 80). The shape of the two curves is almost identical as well as the top angle, reached in both cases around t=0.4 s. A higher bounce is present when the vehicle lands on the ground (t=0.75 s) in the virtual model. Again, it could be due to a different suspension tuning.

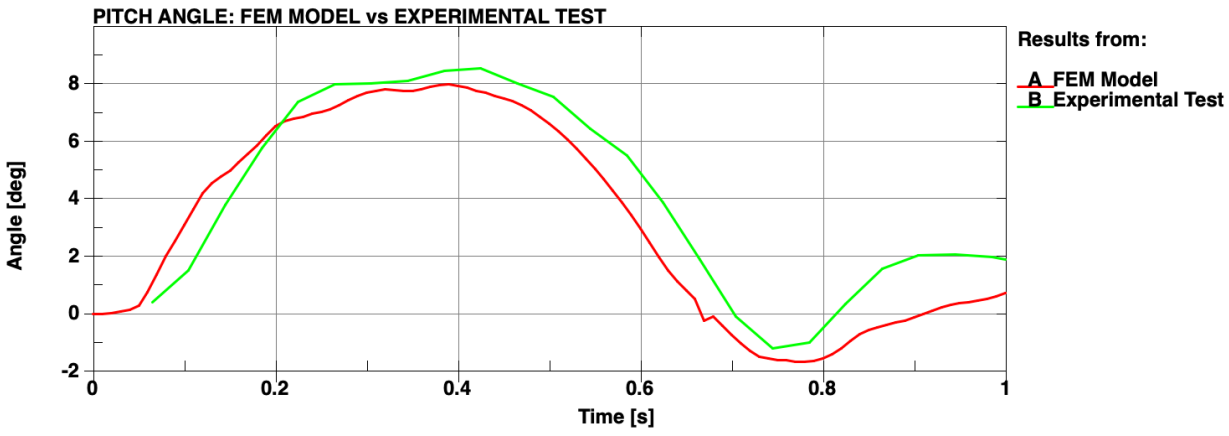

Figure 80. Bollard impact: pitch angle plot

In conlusion, the presented analysis showed a good correlation between the developed virtual model and a real experimental test. Not only the deformation of the front structure is well reproduced, but also the deceleration and the motion of the vehicle during the impact are close enough to confirm the reliability of the N1 model.

It must be considered that the analysis has been carried out setting the virtual model from a video found on the web, and results have been extracted by video processing. The quality of the comparison could be improved knowing the exact dimensions of the vehicle, the suspension tuning, and having access to the data recorded by the accelerometers installed in the real model.

Friction sensitivity analysis

In order to understand the effect of the friction coefficient between vehicle and barrier on the results, a friction sensitivity analysis is performed.

Starting from the model presented in the previous section, with bollard in central position, the following friction coefficients are studied: 0.1, 0.2, 0.3, 0.4, 0.5 (value used in previous simulations), 0.7 and 0.9.

For sake of simplicity, in the following plots, results are divided comparing all the values between 0.1 and 0.5, and then all the values between 0.5 and 0.9. The comparison with the model with friction equal to 0.5 is always present being the value used previously.

The first analysis concerns the impact that friction has on the deceleration of the vehicle. In Figure 81 it possible to see the resultant velocity extracted from Accelerometer 1. Results are filtered using a point average based on 20 points to have a clearer comparison.

The left graph contains the results of the simulations with friction lower than 0.5. It has a clear influence on the first minimum (at t=0.15 s), meaning that lowering the friction coefficient, the deceleration increases. A lower influence is present in following instants of the simulation.

On the right plot, it is possible to notice that values higher than the reference one (0.5) have a lower effect on the deceleration of the vehicle. Increasing the friction coefficient produces a slightly lower deceleration with respect to the reference case.

However, it is possible to notice that the initial trend of all curves (from t=0 s to t=0.1 s) is the same undependably from the friction coefficient.

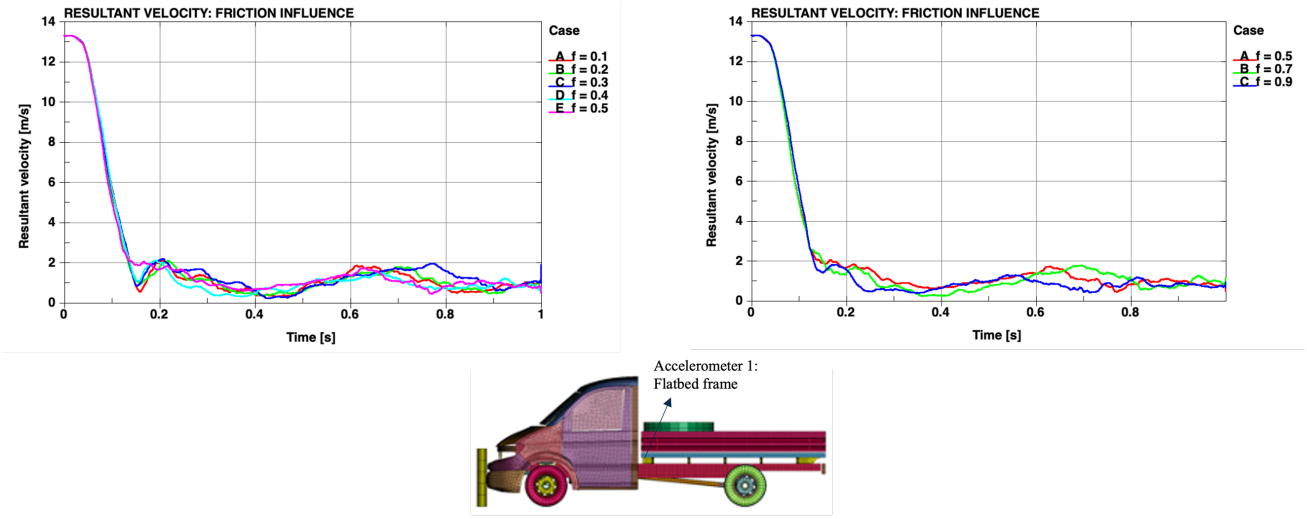

Figure 81. Friction sensitivity analysis: deceleration plots

The second analysis is the influence of friction coefficient on the contact force between vehicle and bollard.

In Figure 82, it is possible to notice that the friction coefficient has a big influence on the contact force only for values lower than 0.5. In particular, the simulation with friction coefficient equal to 0.1 shows the lowest peak. Increasing the value of the parameter, the magnitude of the peak force increases as well, reaching the maximum at f=0.5. Alongside with the first peak, also the secondary peaks change in magnitude and in time.

Increasing the friction coefficient over the reference value, has minor effects, especially on the magnitude of the first peak. Bigger differences can be seen in the secondary peak of the simulation with maximum friction coefficient (0.9).

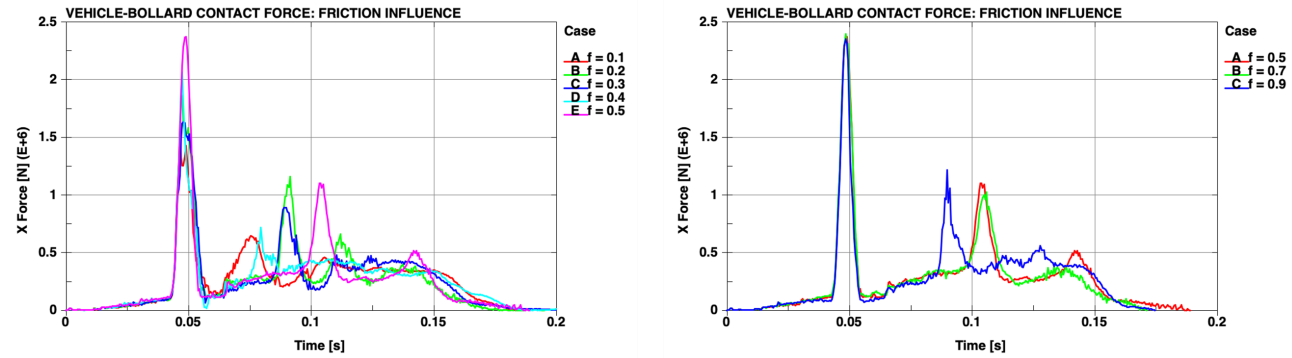

Figure 82. Friction sensitivity analysis: contact force plots

In the previous plots, an alternance of peaks and flat regions is seen in each curve. As shown in Figure 83, where the contact force of the reference case is presented, each peak corresponds to

the impact of the engine against the bollard. Indeed, when the vehicle starts to impact with the bollard, the contact force starts to increase, but the peak is generated only when the engine surface touches the barrier.

After the first peak, the engine block receives a force opposite to its motion and is pushed back creating the flat region. Then, it is pushed against the bollard a second time by the movement of the vehicle, creating the second peak. Being the velocity lower than the first impact, the magnitude of the second peak is lower.

Again, a force is generated on the engine surface that pushes the component in opposite direction, creating a second flat zone. Finally, a third lower peak is generated when the engine contacts again the bollard.

This behavior of the engine bouncing against the bollard several times is seen in all simulations analyzed in this section. The peaks are shifted with respect to the reference simulation because the movement of the engine is different in each case.

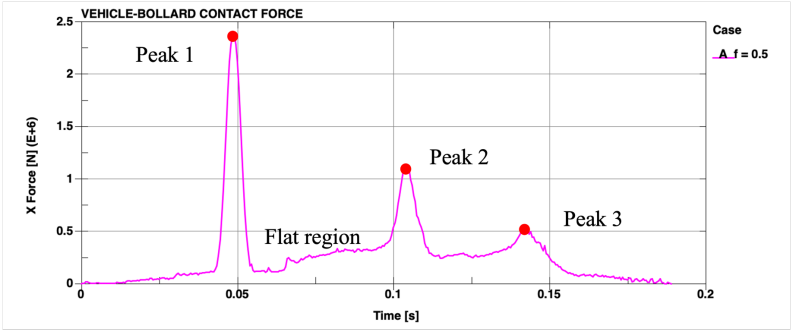

Peak 1 (t=0.05 s):
Engine impact bollard

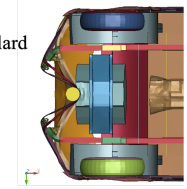

"Flat region" (t=0.05 -0.1s):
Engine bounce back after the first impact

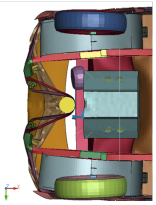

Peak 2 (t=0.1 s):

- Engine impact a second time the bollard
- Peak 3 happens when engine impact a third time

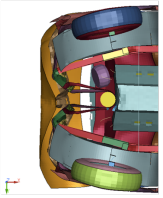

Figure 83. Friction sensitivity analysis: causes of the contact force peaks

To conclude, the friction sensitivity analysis showed a big influence of the friction coefficient only for values lower than 0.5. A negligible impact is present for values higher than the reference one.

Decentered impacts

In a real scenario, it is almost impossible that the vehicle impacts the bollard in a perfectly centered position. It is more probable that the vehicle impacts in a generic position.

In this section, the influence of the position of the bollard is analyzed. In particular, two decentered cases are considered: the first with the bollard aligned with the right longitudinal beam, and the second with the bollard placed in the middle between the centered and the beam-aligned configuration. In Figure 84 it is possible to see the setup of the model with the y-coordinate of the center of the bollard with respect to the global reference system.

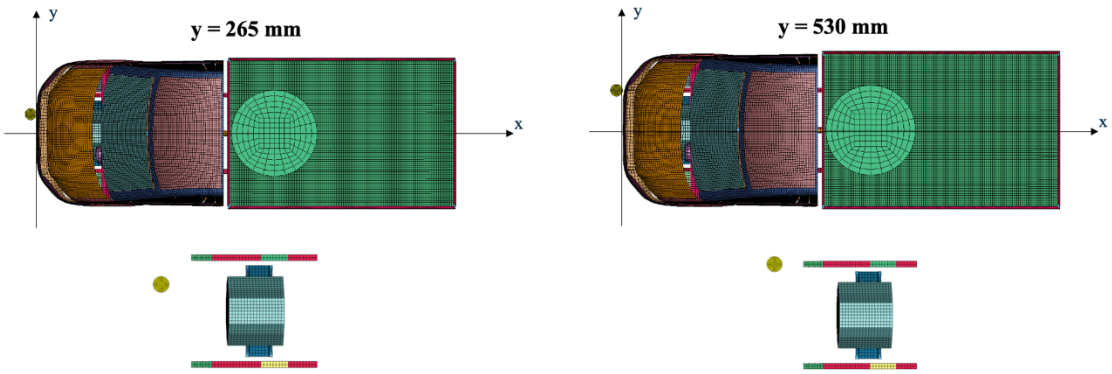

Figure 84. Decentered impact: bollard configurations

The first analysis is the comparison of the animations. In Figure 85 it is possible to see the front view of the simulations at the final instant (t=1 s).

While in the centered case no rotation of the vehicle around the bollard is observed, in the other two cases the model rotates around the bollard axis. As the barrier gets further from the center, a greater yaw rotation is created on the vehicle.

In addition, a different deformation of the tires can be seen. In the reference case they both bend symmetrically inwards, meanwhile in the two decentered cases, a different final position of the tires is seen.

The last evident difference is the deformation of the hood. In the top left image, the bollard causes a higher warping of the component, which stresses the bottom part of the windscreen and causes its rupture in multiple points. In the non-centered model, less deformation of the hood is present, with consequent minor stresses on the windscreen. Only few elements fail in the right part of the windscreen. Finally, in the beam-centered case, the hood has the lowest deformation, and the windscreen has no rupture.

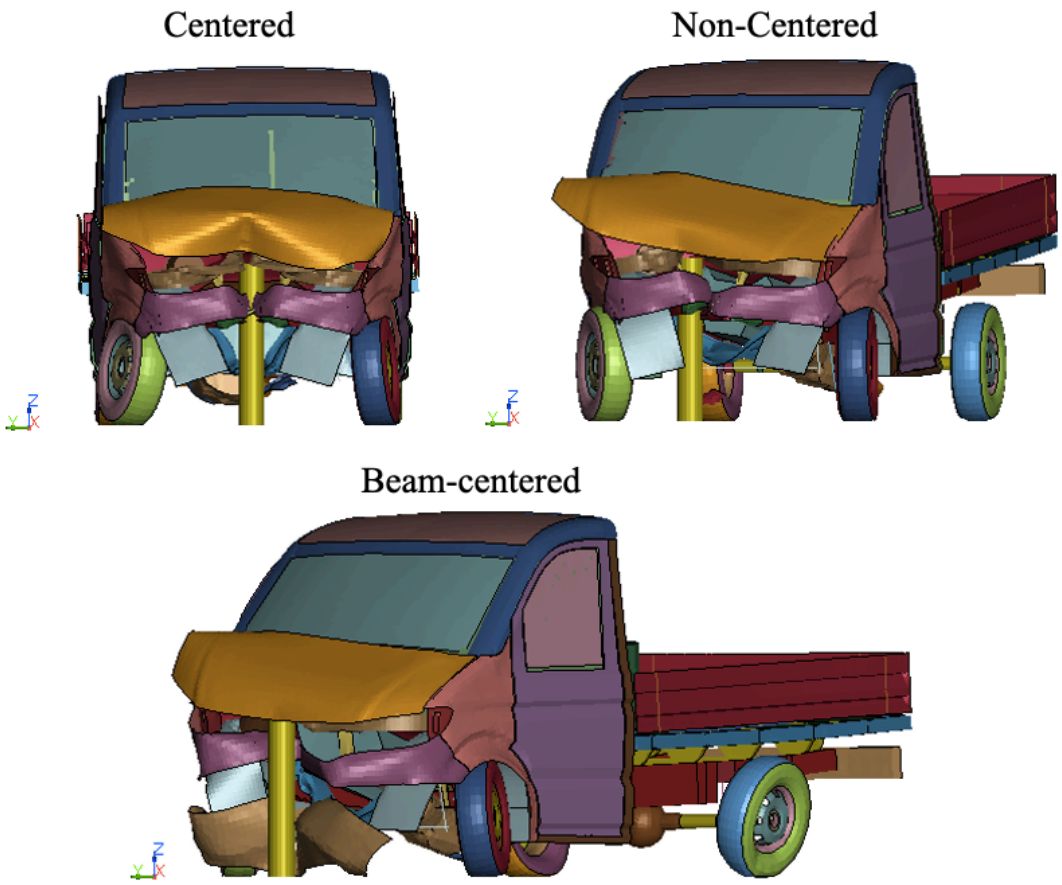

Figure 85. Decentered impacts: front view comparison

Figure 86 shows the bottom view of the simulations at the final instant (t=1 s). The rotation of each model can be better appreciated, and the differences present in the deformation of the tires are more evident.

In addition, it is possible to see the penetration of the bollard inside the front structure of each model. In the centered case the front bumper wrap around the bollard, which penetrates until the engine crossbar. In the non-center impact, the barrier causes the rupture of the bumpers in correspondence of the contact between the two parts.

Finally, in the beam-centered case, the bollard penetrates the front part of the vehicle deforming the front bumper, but the engine crossbar has a lower deformation. This is the only case in which the barrier does not have a contact with the engine front surface. As a consequence, the gearbox crossbar and the transmission do not break during the impact.

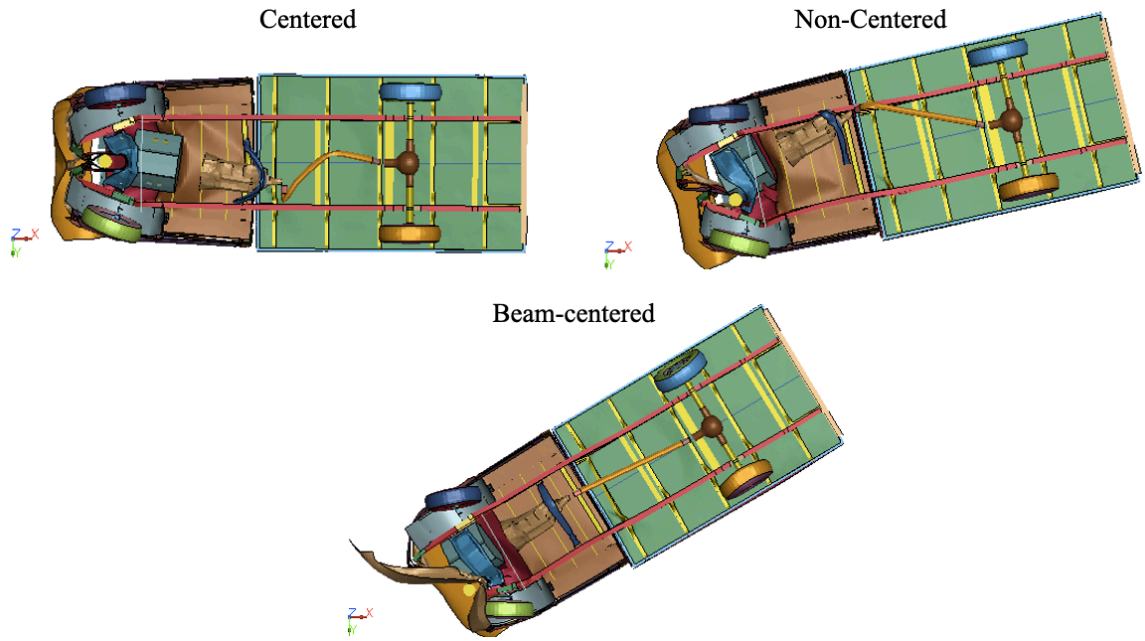

Figure 86. Decentered impacts: bottom view comparison

Analyzing the longitudinal beams, the engine and the bollard from top view (Figure 87), it is possible to the different deformations caused by the barrier. In the left image, both longitudinal beams bend inward, and the engine is impacted at the center of the front surface. In the central image, the bollard causes a bigger deformation of the right longitudinal beam, but a smaller portion of the engine surface is deformed.

Finally, in the beam-centered impact, the bollard slides along the right beams crush zone, and gets stuck between the engine and the right beam. The impact with the engine surface is on its side and the deformation is smaller than in the other cases.

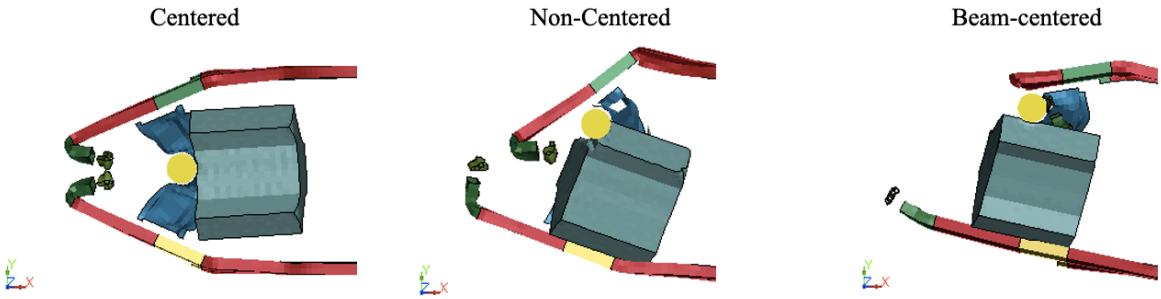

Figure 87. Decentered impacts: frame detail comparison at t=140 ms

Comparing the resultant velocity curves of the 3 cases extracted from Accelerometer 1 (Figure 88), it is possible to see the influence of the position of the bollard on decelerations. While the non-centered impact is well overlapped to the centered case velocity, the beam-centered

simulation has a different trend especially in the very first instants (0-0.1 s). In addition, the deceleration is lower, due to the rotation of the vehicle around the bollard, which creates a more gradual stop.

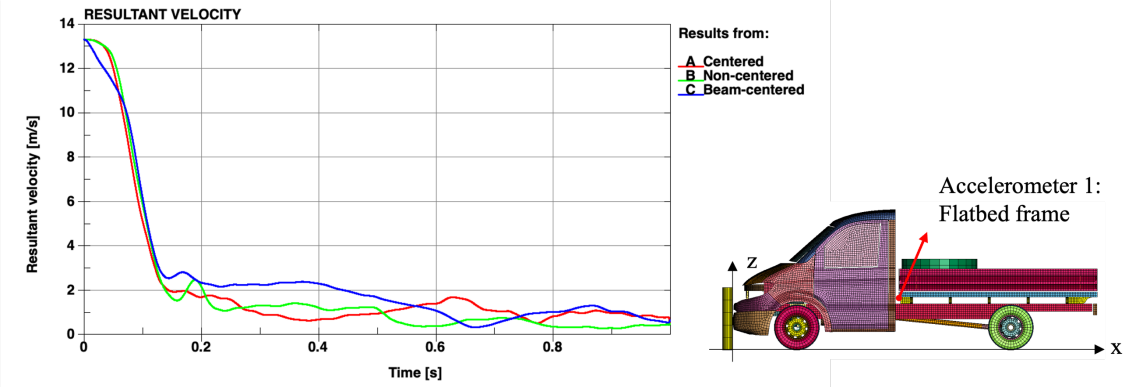

Figure 88. Decentered impacts: resultant velocity plot

For what the contact force is concerned, heavy differences are present in the curves of the 3 cases (Figure 89).

First, the first peak of the X component reduces by half from the centered case to the non-centered case. The beam-centered model does not have a well-defined peak followed by a flat region like in the other simulations. In this case, the maximum of the force is reached later (around t=0.055 s), and its magnitude is lower than the first peak of the non-centered case.

Secondly, as the bollard is moved from the centered position, a Y component arises and becomes relevant. In the right graph, it is possible to see how this component is completely negligible in the reference case, while higher values are reached by the green and blue curves.

However, the resultant contact force is assimilable to the X component because the Y component is lower of one order of magnitude in correspondence of the peaks, and even less in the other regions of the plot.

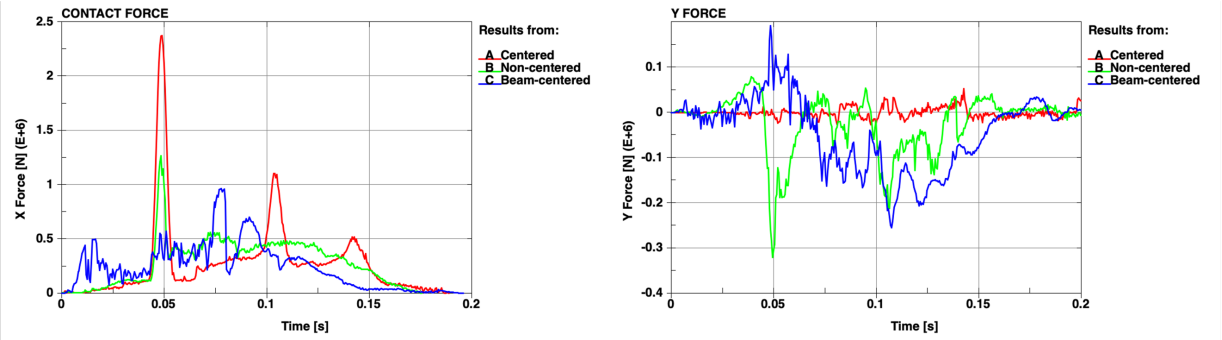

Figure 89. Decentered impacts: contact force plot

As it has been discussed in the friction sensitivity analysis, the impact of the engine on the bollard is the leading cause of the contact force peaks.

In Figure 90, it is possible to see the contact between engine and bollard in correspondence of the contact force peaks. The centered case has the highest peak because the engine impacts at the center and the whole inertia of the vehicle is stopped by this. Secondary peaks are present for the reasons explained in the previous section (Friction sensitivity analysis).

The non-centered case has a lower peak force because the bollard impacts on the edge, and the rotation of the vehicle dissipate part of the energy of the vehicle.

Finally, the beam-centered model has a higher contact force in the first instants (0-0.005 s) because the vehicle starts to be decelerated by the right longitudinal beam, which is stiff enough to slow down the vehicle (while in the other cases, the vehicle didn't stop until the contact between bollard and engine). However, the maximum of the curve occurs in correspondence of the impact between the bollard and the engine side surface.

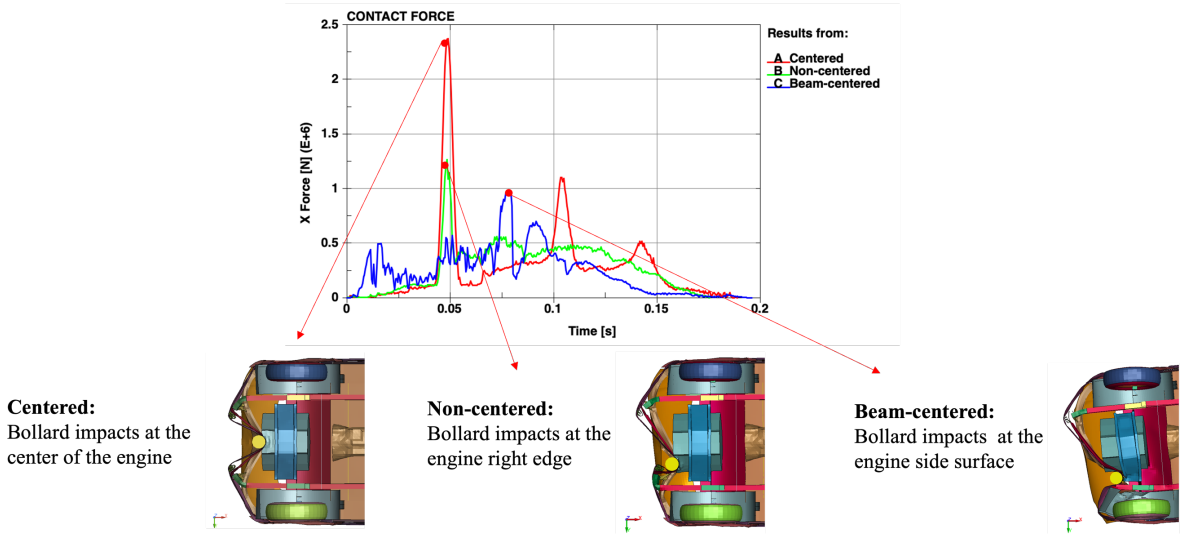

Figure 90. Decentered impacts: contact force peaks explanation

In conclusion, the present section demonstrated the big influence that the position of the bollard has on the behavior of the vehicle and on the contact forces. As the barrier is moved further from the center, a greater rotation around z-axis is caused to the vehicle, and a different deformation of the bumper is seen.

Finally, the importance of the engine on the contact force has been proven once again, showing the different trends created by the different positions of the impact.

Reactions computation

Foundations are one of the most important parts of barriers, because they are needed to correctly anchor the barrier to the ground and avoid its detachment during a vehicle impact. In order to design the foundations, the reaction forces and moments generated at the barrier-ground interaction are needed.

In this final section, a methodology developed to compute reactions of barriers is presented.

To this aim, a new part is appositely created. It consists of a rigid circle made of shell elements which is fixed in all directions. The bollard is fixed with a tied contact to the rigid circle. This new part is added because, generally, it is not possible to choose a section on which compute reactions when using a rigid material. They are generally computed on the whole part. In this way, the forces are transmitted from the bollard to the rigid circle, and the reactions are obtained at a controllable height.

In the present section, the rigid circle is immersed in the ground (Figure 91), to compute the reaction forces needed for designing the foundations.

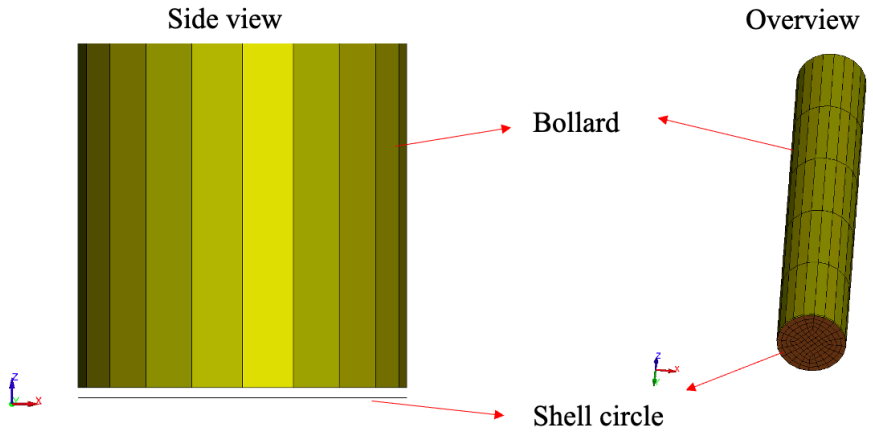

Figure 91. Reactions computation: bollard setup

The methodology is used on the bollard central impact simulation shown in the first section of the present chapter.

The reaction force X component is presented in Figure 92. As in the contact force plots, peaks are present in correspondence of the instants at which the engine impacts the bollard. Again, flat regions are observed when the engine bounce back.

While the first peak of the reaction force is perfectly overlapped to the first peak of the contact force (Figure 93), the magnitude of the secondary peaks is around 50% higher for the reaction force. However, the overall trend is the same for the two forces.

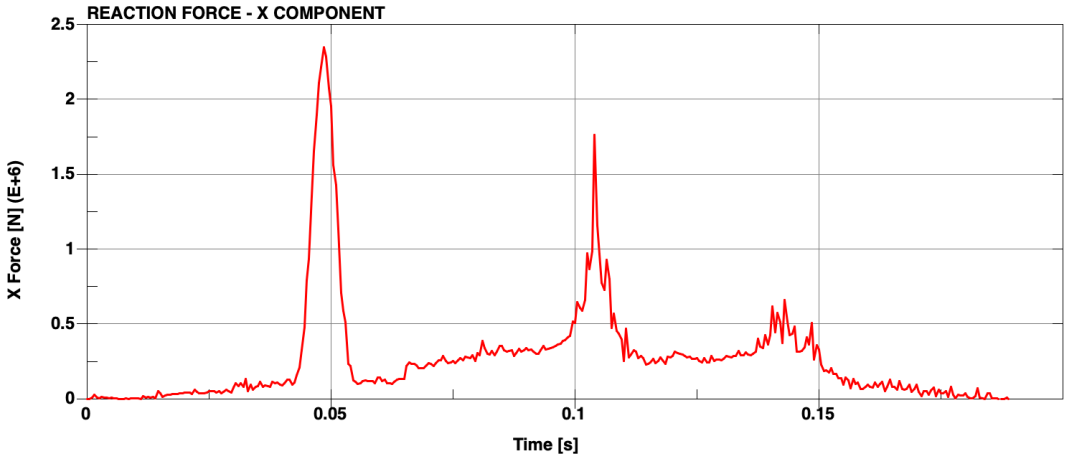

Figure 92. Reactions computation: reaction force X component

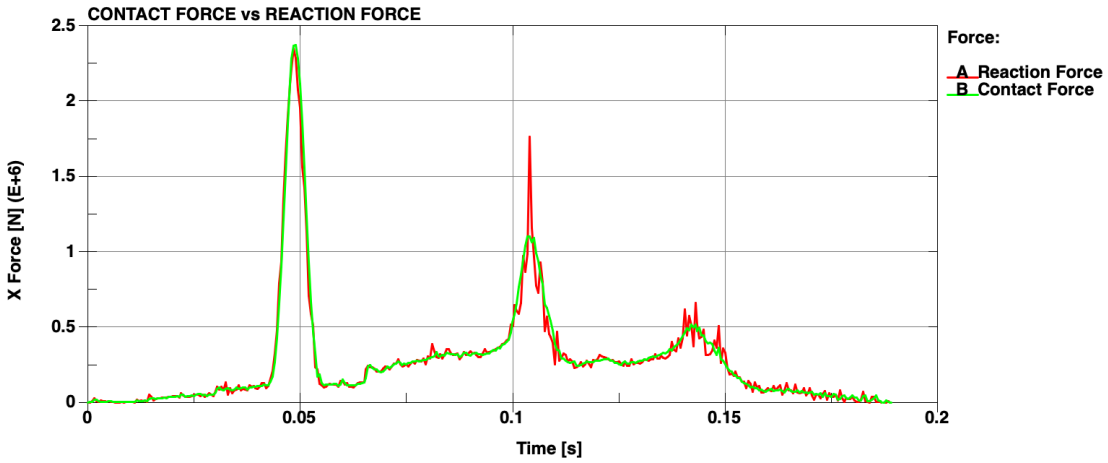

Figure 93. Reactions computation: reaction force vs contact force

The reaction moment computed around y-axis is shown in Figure 94. It is possible to notice that in this case only the first peak is present. It occurs at the same time of the reaction force peak. The remaining part of the graph is almost flat and with values ranging between 0 and 0.1 Nm.

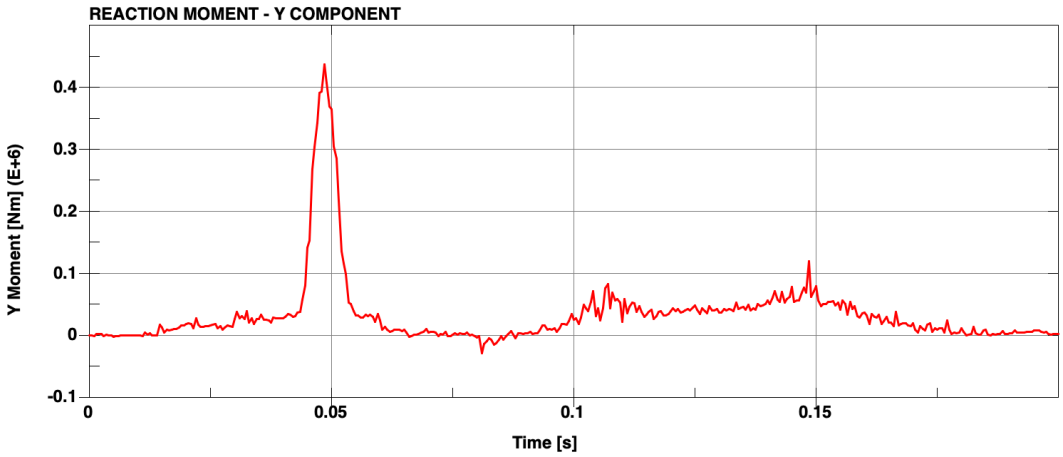

Figure 94. Reactions computation: reaction moment Y component

Presented results are computed at the height of the ground, because the reaction forces are needed as input to correctly design the foundations. However, changing the position of the shell circle, it is possible to obtain the reactions of every section of the bollard.

Conclusions

In the present thesis the reliability of a generic N1 vehicle model created for testing barriers for public spaces protection has been demonstrated performing two sensitivity analysis with a planar rigid barrier and a model validation with a bollard crash test comparison with a real experimental test.

The first analysis demonstrated that the angle between vehicle and barrier has a deep influence on the exchanged energies, forces and momentum as well as on the overall behaviour of the vehicle. Different deformation configurations are observed in the longitudinal beams, both in the central and front part. These differences affect the contact force Y component.

On contrary, the study performed on the influence of friction coefficient demonstrated its poor effects on results.

Then, in the second chapter, the cargo has been positioned in different points of the flatbed to understand its influence during the impact. While energies, forces and momentum are not affected by its position, the deformation of the longitudinal beams is heavily influenced, especially when the mass is placed at the end of the flatbed. In these models a different behaviour of the vehicle is present after the impact with respect to the cases with cargo placed at the centre of the flatbed and near the cabin. Indeed, the vehicle does not settle after the crash, but gains an increasing acceleration which pulls the vehicle in opposite direction with respect to the initial one.

Performed tests demonstrated that the longitudinal beams and the relationship between the cargo and the flatbed floor are the main causes behind this phenomenon.

In the last chapter the N1 model has been validated with a bollard crash simulation reproducing an experimental test of which only the video was available.

Adopting the same bollard and vehicle dimensions used for the model validation, a sensitivity analysis showed the importance of the position of the bollard during the impact, and the main role covered by the engine in the contact force.

Finally, a methodology to obtain reaction forces and reaction moments from a rigid barrier has been successfully developed and can be used with barriers of any type.

References

[1] European Commission's Joint Research Centre, <https://joint-research-centre.ec.europa.eu/index_en>

[2] Generic vehicle model N1, <https://counterterrorism.jrc.ec.europa.eu/generic_vehicle_models.php>

[3] 2023, SVS FEM s.r.o., Všechna práva vyhrazena, <https://www.svsfemservices.cz/>

[4] Sebik, M., Popovic, M., Kleteckova, K., Generic vehicle model N1, European Commission, Ispra, 2022, JRC130165

[5] LIVERMORE SOFTWARE TECHNOLOGY (LST), LS-Dyna R13 Keyword user's manual, vol. 1, AES, 2021

[6] The Engineering ToolBox, accessed 9 November 2022, <https://www.engineeringtoolbox.com/friction-coefficients-d_778.html>

[7] 2023, DYNAmore GmbH, DYNAmore Swiss GmbH, DYNAmore Italia S.r.l., <https://www.dynamore.de/en/products/pre-and-postprocessors/prepost>

[8] Department for transport, Safety of Loads on Vehicles, Third edition, Crown Copyright, 2002, Page 40, accessed 15 November 2022, <https://assets.publishing.service.gov.uk/government/uploads/system/uploads/attachment_data/file/857507/safety-loads-on-vehicles.pdf>

[9] Permissible maximum weights of lorries in Europe, accessed 15 November 2022, <https://www.itf-oecd.org/sites/default/files/docs/weights-2019.pdf>

[10] FIAT Professional, Ducato Conversion, <https://www.fiatprofessional.al/model/ducato-conversion/#:~:text=maximum%20permitted%20axle%20loads%3A%20up,the%20rear%2C%20segment%20topping%20values>

[11] Crash test borne fixe ALE F16-100-C50, AMCO LES ESCAMOTABLES, <https://www.youtube.com/watch?v=0xfZEso0dxM>

[12] Douglas Brown, Wolfgang Christian, Robert M Hanson, Tracker: Video analysis and modelling tool, OSP, comPADRE, GNU, 2023

[13] ALE F16-100-C50, AMCO LES ESCAMOTABLES, <https://assets.ctfassets.net/wutvz7hlq4gn/3X57kv4d3RlT2zS1qmP973/53607f7cf513345bfad3ba7cd345b5ca/FT_ALE_F16-100-C50.pdf>